

DESIGN OF A NON-SNAGGING GUARDRAIL POST

A Thesis

Submitted to the Faculty

of the

Worcester Polytechnic Institute

in partial fulfillment of the requirements for the

Degree of Master of Science

in

Civil Engineering

by

Jessica Elisabeth Karlsson
June 2000

Approved:

Dr. Malcolm H. Ray, Major Advisor

Dr. Frederick L. Hart, Department Head

ACKNOWLEDGEMENTS

This thesis is a partial requirement for a degree of Master of Science in Civil Engineering and was performed at Worcester Polytechnic Institute in Worcester.

I would like to thank my advisor Professor Malcolm Ray at Worcester Polytechnic Institute for his excellent support during the work and also for giving me the opportunity to perform my thesis work at Worcester Polytechnic Institute. I would also like to thank Research Associate Chuck Plaxico at Worcester Polytechnic Institute for guidance and advice during the work.

Finally, I would like to thank Professor Larsgunnar Nilsson at Linköping University in Sweden for establishing the contact that made this thesis work possible.

Jessica Karlsson
Worcester, June 23, 2000

ABSTRACT

The purpose of this project is to design a non-snagging guardrail post. The procedure will be to first develop a simple finite element (FE) model of a single post, wheel and suspension to explore the snag potential for some existing standard guardrail posts. The next step in the procedure will be to develop appropriate design changes that could prevent wheel snagging and investigate if they do by using a one-post sub-model. An attempt to validate the used material model for wood will also be done by comparison between laboratory tests and finite element simulations.

TABLE OF CONTENTS

1. INTRODUCTION	1
2. LITERATURE REVIEW	3
2.1 Full-scale Crash Tests	3
2.2 Post component test reports	6
2.3 Finite Element modeling reports.....	7
3. RESEARCH PLAN	12
3.1 Timber Material.....	12
3.2 Simple One-Post Sub-Model.....	13
3.3 Post Alternatives	13
3.4 Finite Element Analysis of Alternatives using the Sub-Model.....	13
4. TIMBER MATERIAL.....	14
4.1 Laboratory Tests	14
4.2 FE Modeling.....	19
4.3 Comparison and Validation.....	22
5. SIMPLE ONE-POST SUB-MODEL.....	25
5.1 Lateral Loading.....	25
5.2 Wheel-Post Contact.....	34
6. POST ALTERNATIVES	45
6.1 Deeper Block-outs.....	45
6.2 Longitudinal Failure Fuses	46
6.3 Lateral Failure Fuses.....	46
6.4 Different Cross-sections.....	47
7. FINITE ELEMENT ANALYSIS OF ALTERNATIVES.....	48
7.1 Deeper Block-outs.....	48
7.2 Longitudinal Failure Fuses	57
8. RESULTS.....	72
9. CONCLUSIONS.....	73
10. REFERENCES.....	75

LIST OF FIGURES

Figure 1. Full scale test showing wheel snagging. (6).....	1
Figure 2. Deflection versus time for dynamic bogie test with timber post. (15)	7
Figure 3. Sketch of laboratory test set-up.	15
Figure 4. The laboratory test set-up.	15
Figure 5. The wood support on each side of the specimen.	16
Figure 6. Typical failure of the tested wood specimens.....	16
Figure 7. Deflection versus time for the laboratory test performed on wood specimens.	17
Figure 8. Force versus time for the laboratory tested wood specimens.	18
Figure 9. Energy versus time for the laboratory tested wood specimens.....	18
Figure 10. The model used in the validation of wood material model.....	20
Figure 11. Deflection versus time for the model used in the material validation for wood.	21
Figure 12. Force time history for the model used in the material model validation.	21
Figure 13. Internal energy time history for the model used in the material model validation.	22
Figure 14. Deflection versus time comparison between laboratory test and FE model....	23
Figure 15. Force time history comparison between laboratory tests and FE model.	23
Figure 16. Energy time history comparison between laboratory tests and FE model.....	24
Figure 17. Standard 150x200 mm grade 2 wood post struck by a 1400 kg cylindrical impactor at 32 km/hr.	27
Figure 18. Maximum deflection of a steel W150x13.5 post showing a lateral torsional buckling failure.	29
Figure 19. Deformation of a steel W150x13.5 post showing a lateral torsional buckling failure. (6).....	29
Figure 20. Steel W150x23.5 post struck by a 1400 kg cylindrical impactor at 32 km/hr.	30
Figure 21. Force time history for the different posts bent by a cylindrical striker (100 point running average filter).....	31

Figure 22. Post strain energy time history for the different posts bent by the cylindrical striker.....	32
Figure 23. Energy absorbed by the soil for the different posts.	33
Figure 24. Sketch showing how the wheel is positioned related to the post.....	35
Figure 25. Wheel snagging on standard 150x200 mm grade 2 wood post.	36
Figure 26. Steel W150x13.5 post and wheel.....	37
Figure 27. Steel post W150x23.5 and wheel that snag.	37
Figure 28. The model with the wheel attached to a block.....	40
Figure 29. The steel W150x13.5 post assembled with the wheel with vehicle inertia.	41
Figure 30. Resultant joint force versus time for 150x200 mm wood post and steel W150x13.5 post (filtered to SAE 60).....	42
Figure 31. The impulse delivered to the wheel for the 150x200 mm wood post and the steel W150x13.5 post.	43
Figure 32. Sketch showing deeper block-out.....	45
Figure 33. Sketch showing post with longitudinal failure fuses.	46
Figure 34. Sketch showing post with lateral failure fuses.....	47
Figure 35. Definition of overlap.....	48
Figure 36. Wood post with block-out depth 250 mm, which prevent wheel from snagging.	49
Figure 37. The overlap variation against the block-out depth for wood post.	50
Figure 38. Resultant joint force versus time for different block-out depths (filtered to SAE 60).....	51
Figure 39. Resultant peak joint force variation for different block-out depths.....	51
Figure 40. The resultant joint force curves subtracted by the joint force curve for the block-out depth 250 mm (filter to SAE 60).	53
Figure 41. The impulse delivered to the wheel at the different block-out depths after the 250-mm block-out depth curve is subtracted.	54
Figure 42. The block-out depth versus the impulse delivered to the wheel.....	55

Figure 43. Comparison between resultant joint forces on the wheel for wood post modeled with and without failure for a block-out depth of 50 mm (filtered to SAE 60).....	57
Figure 44. Model of the CRT timber post.....	58
Figure 45. Sketch showing coordinate system used in calculations of mass moment of inertia.....	59
Figure 46. CRT post failure caused by lateral loading.....	60
Figure 47. Deflection time history for the CRT post.	61
Figure 48. Force time history for the CRT post and for the standard wood post as comparison (100 point running average filter).....	61
Figure 49. Post strain energy time history for the CRT post and for the 150x200 mm wood post as comparison.	62
Figure 50. CRT post failure caused by wheel impact.	63
Figure 51. The resultant joint forces versus time for the CRT post (filtered to SAE 60).	64
Figure 52. The impulse delivered on the wheel for the CRT post.	65
Figure 53. Post with one hole above ground line.....	66
Figure 54. Force time history for the post with one hole above ground bent by cylindrical striker (100 point running average filter).	67
Figure 55. Post strain energy time history for the post with one hole above ground line.	68
Figure 56. Failure of post with one hole above ground caused by wheel contact.	69
Figure 57. Resultant joint force versus time for the post model with one hole above ground line (filtered to SAE 60).....	70
Figure 58. Impulse delivered to the wheel in the model with the post with one hole above ground line.....	70

LIST OF TABLES

Table 1. Results from full-scale tests. (4).....	4
Table 2. Results from dynamic bogie impact tests. (14).....	6
Table 3. Wood post material properties used in LS-DYNA analysis. (9).....	8
Table 4. Timber material properties. (10).....	9
Table 5. Received data from laboratory tests performed on wood specimens.....	17
Table 6. Properties used in the FE model of wood specimen for validation of material model.	19
Table 7. Simulation runtime statistics for wood material validation model.	20
Table 8. Post and soil properties used in the model of the wood post.	26
Table 9. Simulation statistics for the standard 150x200 mm wood post sub-model.....	27
Table 10. Properties used in the steel post model.	28
Table 11. Simulation statistics for the steel W150x13.5 mm and the steel W150x23.5 post sub-models.....	30
Table 12. Simulation statistics for the standard 150x200 mm wood post sub-model with wheel contact.	36
Table 13. Simulation statistics for steel posts, W150x13.5 and W150x23.5 post sub-models with wheel.	38
Table 14. Simulation statistics for wood post sub-model with wheel attached to a block.	40
Table 15. Simulation statistics for steel W150x13.5 post sub-model with wheel attached to a block.....	41
Table 16. The calculated mass moment of inertia for standard wood post and CRT post.	58
Table 17. Simulation statistics for the modeled CRT post exposed to lateral loading.	60
Table 18. Simulation runtime statistics for the CRT post exposed to wheel contact.....	64
Table 19. Simulation runtime statistics for the post with one hole above ground exposed to wheel contact.	66

Table 20. Simulation runtime statistics for the post modeled with one hole above ground wheel with vehicle inertia.....	69
Table 21. Comparison between results for the different types of wood posts.....	71

1. INTRODUCTION

Strong post guardrails sometimes “snag” the wheels of some vehicles like pickup trucks, sport-utility vehicles (SUV) and small cars during collisions as shown in Figure 1.



Figure 1. Full scale test showing wheel snagging. (6)

This often causes stability problems or tears the wheel off the vehicle resulting in the vehicle rolling over or spinning out. It can also cause high decelerations, which in turn may cause occupant injuries. Typical posts used today in strong post guardrails are a 150x200 mm wood post, a 200x200 mm wood post and a W150x13.5 steel post. When the post bends over in the soil the wheel can get caught on the post resulting either in the vehicle rolling over or the loss of the wheel. A post that is designed to deform or breakaway such that the wheel cannot directly contact the post would prevent vehicles from snagging and would therefore improve the performance of many guardrail systems.

The objective of this thesis is to develop a non-snagging guardrail post by using finite element simulations. Different alternatives will be developed and then the snag potential of the new designs will be investigated. Some laboratory tests will also be performed to validate the used material model for wood in the FE simulations.

2. LITERATURE REVIEW

The following reports and papers deal with aspects of wheel snagging on strong post guardrails during collision.

2.1 Full-scale Crash Tests

Ivey, Robertson and Buth performed full-scale crash tests with conventional W-beam and thrie-beam guardrail systems that were impacted by heavy vehicles like school buses. (3)

The report also describes the development and evaluation of a modified thrie-beam guardrail. Two tests were done with a 9081 kg bus, one with the speed of 89.5 km/hr and 13.5 degree impact angle and one with the speed of 96.0 km/hr and 15.0 impact angle.

The tests resulted in one 90 degree roll over and one penetration into the zone behind the rail, which lead to a complete roll over, partly because of snagging. Both results were unacceptable and significant design changes had to be made to get a guardrail that would safely contain and redirect a bus. The changes that were made were to increase the height of the barrier, increase the block-out depth to 360 mm, make a triangular shaped notch on the web, increase the embedment length and change to a thrie-beam guardrail. This modified guardrail was tested with a 9081 kg bus at 89.8 km/hr and 15 degree impact angle. It resulted in a stable, acceptable collision. Two tests were also done with 1032 kg Honda Civics impacting the rail at 100.6 km/hr and 15 degrees and 99.1 km/hr and 18.0 degrees, respectively. The results from both tests were considered satisfactory and no snagging was observed. A final test was performed to see if the modified guardrail could redirect a 14515 kg intercity bus at 60 km/hr and 14 a degree impact angle. The overall

reaction of the bus could be termed ideal. In summary, no snagging was observed when the block-out size was increased to 360 mm.

Stout, Hinch and Yang created and validated a post-soil interaction model and performed full-scale tests of strong-post guardrails with standard and non-standard installations. (4) Two systems were tested in the standard configuration and with a 2134 mm post. The posts were installed at the breakpoint of a 2:1 foreslope. Four tests were done and the results that can be seen in Table 1 show that one of the tests resulted in wheel snagging.

Test	Guardrail type	Length (mm)	Speed (km/hr)	Impact angle	Results
1717-1-88	G4(1S)	2134	97.6	26°	No redirection, penetration into rail
1717-2-88	G4(1S)	1829	97.9	27°	Redirection, rollover, penetration into rail
1717-3-88	G2	2134	97.3	25°	Redirection, too high speed change
1717-4-88	G2	1600	97.9	26°	Redirection, penetration into rail, snagging

Table 1. Results from full-scale tests. (4)

A full-scale test with a 2000 kg pickup truck impacting a weak-post W-beam (G2) guardrail system where snagging was observed was performed and investigated by Mak and Alberson. (5) The truck had a speed of 71.0 km/hr and an impact angle of 26.1 degrees and snagging was observed.

Mak and Menges did crash testing and evaluation of strong-post W-beam guardrail systems impacted by a 2000 kg pickup truck at 100 km/hr and 25 degrees. (6) Two test installations were tested, the standard G4(2W) guardrail system and the standard G4(1S) guardrail system. In the first test with the G4(2W) system the left front wheel snagged and separated from the vehicle. The test performed with the G4(1S) system resulted in left front tire snagging and the vehicle began to spin out into the traveled way. When contact between vehicle and rail ended the vehicle rolled onto its side. The maximum dynamic deflection at guardrail height was 866 mm for the 150x200 wood post.

Mak and Menges performed two full-scale crash tests with the thrie-beam guardrail system and a 2000 kg pickup truck as test vehicle. One was with the modified thrie-beam guardrail and one was with the thrie-beam (G9) guardrail. (7) (8) In the test performed with the modified thrie-beam guardrail system the left front wheel snagged and then the wheel assembly was torn from the vehicle's axle. The test with the thrie-beam guardrail system resulted in wheel snagging and vehicle rollover. Both of the tests were performed at a nominal speed and impact angle of 100 km/hr and 25 degrees.

The above reports and papers show examples of snagging and what happens when the vehicle wheel snags. This is useful in knowing what kind of existing guardrail posts and block-outs are associated with snagging. The deflection and other results from the full-scale crash tests are used in making a realistic behavior of the post in the FE modeling.

2.2 Post component test reports

Coon, Reid and Rohde did a dynamic impact testing of steel and wooden guardrail posts embedded in soil. (14) The posts tested were W150x13.5 steel posts, W150x23.5 steel posts and 150x200 Southern Yellow pine posts. The W150x23.5 posts were tested in order to isolate the failure in the soil by using a post that does not deform in a typical impact. The posts were impacted with a bogie vehicle with a mass of 946 kg at velocities of 5.5, 8.9 and 13.4 m/s. Results from the tests are shown in Table 2.

Type of post	Impact velocity (m/s)	Peak force (kN)	Maximum deflection (mm)	Resulting bogie condition
Steel post:				
W150x13.5	4.6	64.0	234	Stopped
W150x13.5	6.0	32.3	597	Stopped
W150x13.5	5.4	66.9	314	Stopped
W150x13.5	5.9	67.0	348	Stopped
W150x23.5	8.9	104.7	597	Ride over
W150x23.5	8.9	86.3	597	Ride over
Wood post:				
150x200 mm	4.9	36.3	444	Stopped
150x200 mm	4.8	38.8	450	Stopped
150x200 mm	9.6	77.8	597	Stopped
150x200 mm	9.0	64.2	145	Post fracture

Table 2. Results from dynamic bogie impact tests. (14)

Holloway, Bierman, Pfeifer, Rosson and Sicking performed dynamic bogie tests on timber and steel posts in clay and sandy soils and with varying soil moisture contents and then they used the test data to evaluate a computer simulation. (15) The bogie that was used in the dynamic tests weighed 1390 kg and had an impact velocity of around 32

km/hr. The deflection-time results for the 150x200 mm timber post is shown Figure 2. As shown in Figure 2, the maximum post deflection was approximately 500 mm at the ground line.

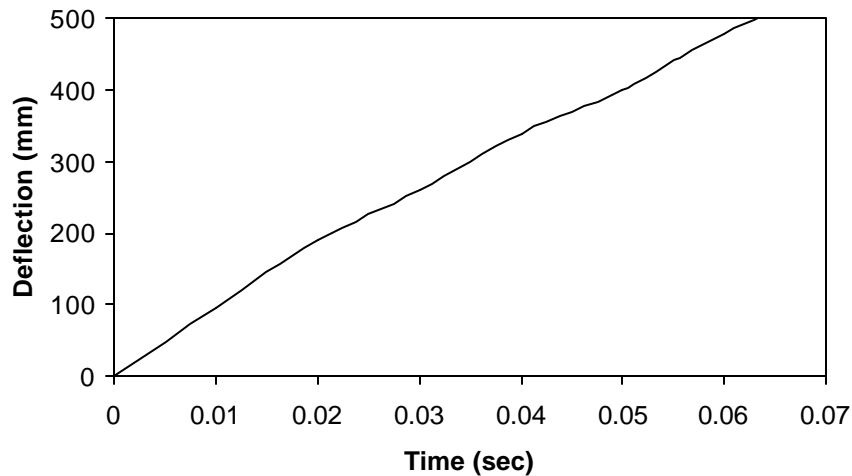


Figure 2. Deflection versus time for dynamic bogie test with timber post. (15)

The results from the dynamic tests from these reports above will be useful in developing a realistic model of the post in a typical impact.

2.3 Finite Element modeling reports

Ray and Patzner developed a finite element (FE) model using LS-DYNA3D of the modified eccentric loader terminal (MELT). The model was used to investigate the performance of the MELT when struck by a 2000P pickup. (9) Wood posts were modeled using solid elements and a combination of different material models. The region where failure will occur is modeled with material type 13 (elastic-plastic material with failure) using the 14-point integration element formulation. The top portion of the post is

modeled with material type 1 (elastic material model) to keep the simulation time as short as possible. The rest of the post is modeled with material type 3 (kinematic-isotropic elastic-plastic material model). The wood post material properties used in this analysis are shown in Table 3.

Element type	BT	Solid
Density	610	kg/m ³
Poisson's ratio	0.30	
Upper portion:		
Material type	1	Elastic
Mod. of elasticity	11	GPa
Failure region:		
Material type	13	Isotropic-elastic-plastic with failure
Shear modulus	4231	MPa
Bulk modulus	9167	MPa
Yield stress	27	MPa
Failure pressure	-120	MPa
Below ground line:		
Material type	3	Isotropic-elastic-plastic
Mod. of elasticity	200	GPa
Yield stress	40	MPa

Table 3. Wood post material properties used in LS-DYNA analysis. (9)

A finite-element model of a guardrail system with timber posts and the post-soil interaction was performed by Plaxico, Patzner and Ray. (10) Also in this model different material models were used depending on which part of the post that were modeled. The properties and material types that were used can be seen in Table 4.

Non-failing region:		
Material type	3	Isotropic-elastic-plastic
Element type	solid	1-point integration
Density	610	kg/m ³
Mod. of elasticity	11	GPa
Poisson's ratio	0.3	
Yield stress	40	MPa
Tangent modulus	11	MPa
Failure region:		
Material type	13	Isotropic-elastic-plastic with failure
Element type	solid	14-point integration
Density	610	kg/m ³
Poisson's ratio	0.3	
Shear modulus	4231	MPa
Bulk modulus	9167	MPa
Yield stress	40	MPa
Failure pressure	-90	MPa

Table 4. Timber material properties. (10)

An array of uncoupled springs was used to support the guardrail posts. The springs represent the soil material. Another factor that affect the properties of the modeled soil is the angle of internal friction, ϕ , that is changed for different soil types and densities. The angle in this model was changed until the simulation results agreed with physical pendulum tests. That occurred for an angle of 35 degrees.

The effect of post and soil strength on the performance of the modified eccentric loader breakaway cable terminal (MELT) has been investigated by Patzner, Plaxico and Ray.

(11) The modeling of the post-soil interaction and the material model for modeling wood

have been done the same way as in the latest discussed report above. The purpose with this report is to establish suitable combinations of post and soil strengths.

Plaxico, Ray and Hiranmayee performed a comparison of the impact performance of the G4(1W) and G4(2W) guardrail systems in a finite-element model and a full-scale test.

(12) A finite element model of the G4(2W) was developed and the results of a simulation of the Report 350 Test 3-11 impact conditions were compared to a full-scale crash test. Once good agreement was achieved between the finite element simulation and the crash test a second finite element model was developed of the G4(1W) guardrail system. These simulations of the two different G4 systems were compared to determine if their performance was similar. The results of the simulations indicated that the two guardrail systems result in essentially identical performance in the Report 350 Test 3-11 conditions. The simulations as well as the full-scale tests show significant wheel snagging.

Sicking and Ross tried to do a structural optimization of a strong-post W-beam guardrail.

(13) The goal of this structural optimization was to maximize the efficiency of every element in the guardrail. The simulation program used was GUARD. The design of a strong-post W-beam guardrail is specified by four basic variables: post spacing, rail height, post size and embedment, and block-out size. Variations of these variables can significantly change the impact performance. The two block-out depths that were considered in this report were 254 and 356 mm. The analysis resulted in that GUARD

predicted that mini-vehicle wheel snag can be prevented with 254 and 356 mm block-out depths.

Since snagging is a serious problem that is often observed in full-scale crash tests the finite element method might be a good way to explore the interaction between post and wheel. In that way the course of event can be predicted and undesired occurrence can be prevented before a full-scale test is performed, which saves both time and money.

3. RESEARCH PLAN

The finite element code LS-DYNA, an explicit three-dimensional non-linear finite element code for analyzing the large deformation dynamic response of inelastic solids and structures, was used in this research. (2) The interactive mesh generator TrueGrid was used to generate meshes for the finite element simulation code. (1) The preprocessor LS-INGRID was also used.

Accomplishing the objectives of this project will involve performing the following tasks:

3.1 Timber Material

Wood is a natural material with different mechanical properties in different directions. It is, therefore, a complex anisotropic material and its properties are dependent on among other things the moisture content and the temperature which makes it even more complex. Those factors make it difficult to predict the behavior on wood and they also make it difficult to develop a wood model that in a simulation corresponds to the real behavior. The purpose of this task is to validate the material model used by LS-DYNA by performing laboratory experiments and then compare them to a FE model developed with the same or as similar conditions as possible.

3.2 Simple One-Post Sub-Model

A simple FE model of just one post, the impacting wheel and the suspension of the vehicle will be developed. It should start by modeling the impact with standard post types that have known test performance. When the simple model replicates the physical tests in the literature the next step is to explore alternative arrangements.

3.3 Post Alternatives

Explore some alternative post designs by using different geometries. Using a deeper block-out is one alternative that is explored in this research and so is also the option is to design a failure mechanism like holes that make the post fail at specific loads. Designing a post that rotates or moves out of the way to avoid snagging or developing new post geometries that will work better is another option. Exploring the use of different materials is yet another option.

3.4 Finite Element Analysis of Alternatives using the Sub-Model

Build FE models of the more promising alternatives and use the simple post-wheel-suspension model from the first task to evaluate the alternatives and decide which ones seem to be the most promising in preventing wheel snagging.

4. TIMBER MATERIAL

Wood, unlike steel, is difficult to model in LS-DYNA since there is no material model that is directly applicable to its behavior. A validation of the material model is, therefore, preferable and is done by comparing dynamic laboratory tests of a wood sample with certain geometry and conditions with a FE simulation with the material model used for wood with the same geometry and conditions as the physical tests.

4.1 Laboratory Tests

The wood specimens that were laboratory tested have the dimension 38.1x38.1-mm and a test length of 304.8-mm. The samples are “clear” wood samples, which means wood that is essentially free from defects. The best wood type to use is “Southern yellow pine” since that is the material that guardrail posts are made of. The tests were performed in a Instron 8250 drop tower. Each end of the specimen rests on a support and the load is applied in the middle such that the beam is subjected to three point bending. A sketch of the test set-up is shown in Figure 3.

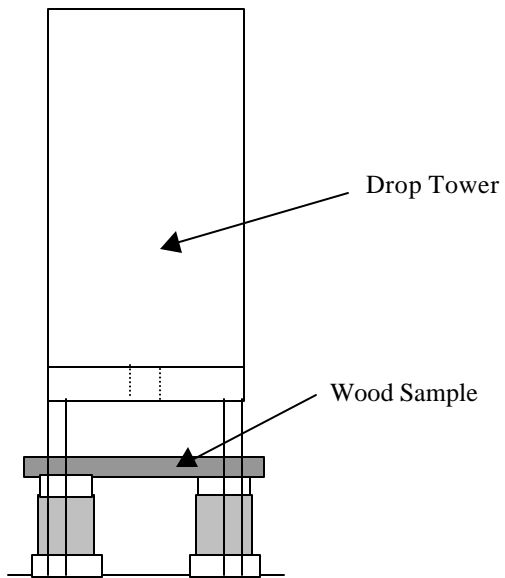


Figure 3. Sketch of laboratory test set-up.

The laboratory test set-up is shown in Figure 4.

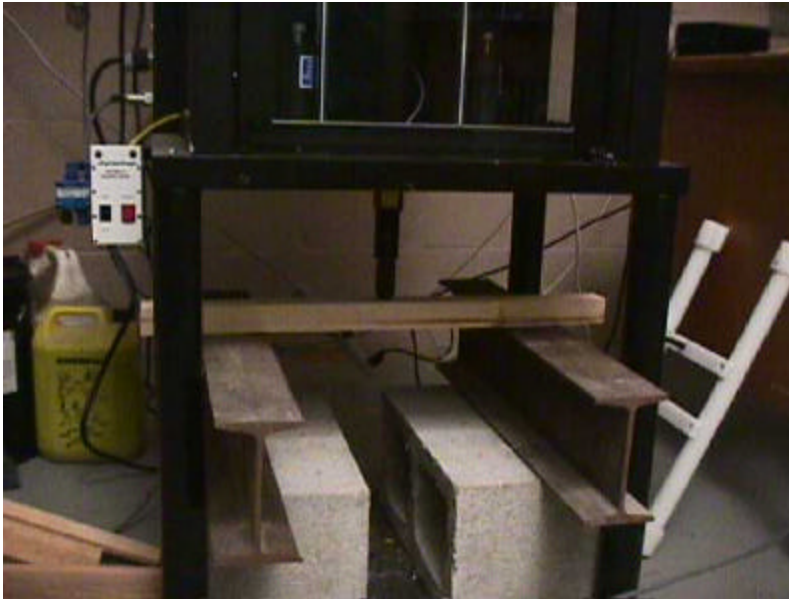


Figure 4. The laboratory test set-up.

To keep the specimen correctly positioned during the impact, a support was inserted on each side of the specimen as shown in Figure 5.



Figure 5. The wood support on each side of the specimen.

The side support does not restrict the specimen in any way except to prevent lateral motion. It is there only to prevent sliding and sideways movement.

Twenty specimens were tested. The failure appearance in the samples was consistent except for a few samples that had small defects like knots at the location where failure should occur. A typical tested specimen showing the failure can be seen in Figure 6.

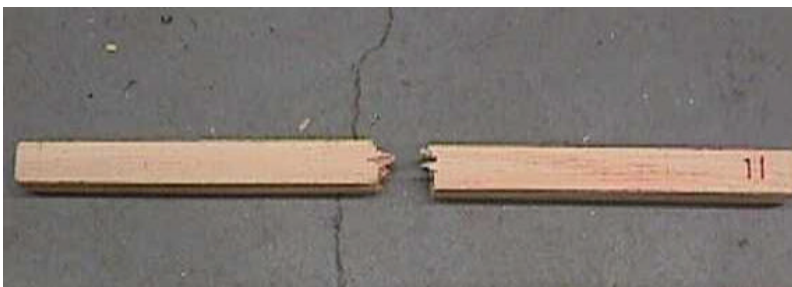


Figure 6. Typical failure of the tested wood specimens.

The maximum, minimum and typical average data from the twenty tests performed are shown in Table 5. The data collected using a 22250 N force sensor tup and the Dynatup data acquisition software.

Type of test	Impact velocity (m/sec)	Impact energy (Nm)	Maximum load (kN)	Energy to maximum load (Nm)	Time to max load (msec)	Deflection at maximum load (mm)
Maximum	3.774	90.100	4.035	35.650	4.722	16.515
Minimum	3.762	89.518	3.172	16.512	2.898	10.626
Average	3.769	89.858	3.510	25.872	3.783	13.539

Table 5. Received data from laboratory tests performed on wood specimens.

The deflection time history for the tests is shown in Figure 7. The deflection time history was identical and did not vary for all the tests shown in the table above. The factor that varies and therefore changes the deflections in the different tests is the time to failure and as can be seen in the table above. The deflection at maximum load varies between approximately 11 mm and 17 mm.

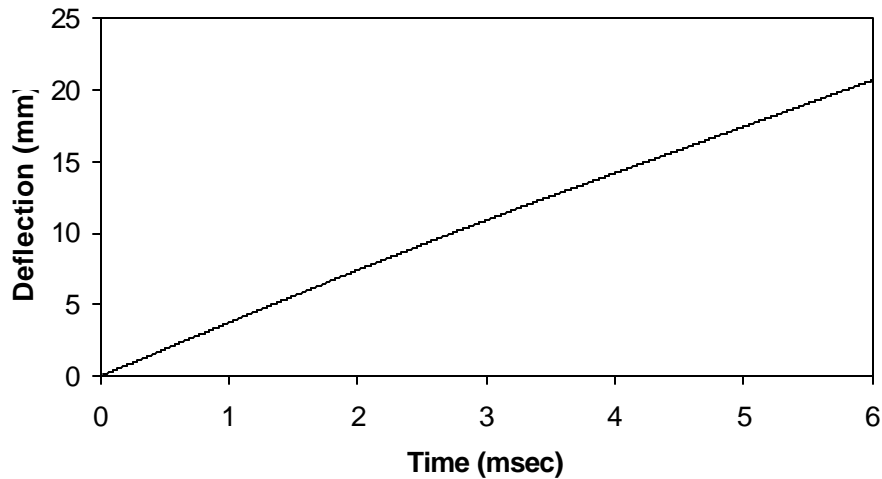


Figure 7. Deflection versus time for the laboratory test performed on wood specimens.

In Figures 8 and 9 the maximum, minimum and a typical average force and energy histories are shown.

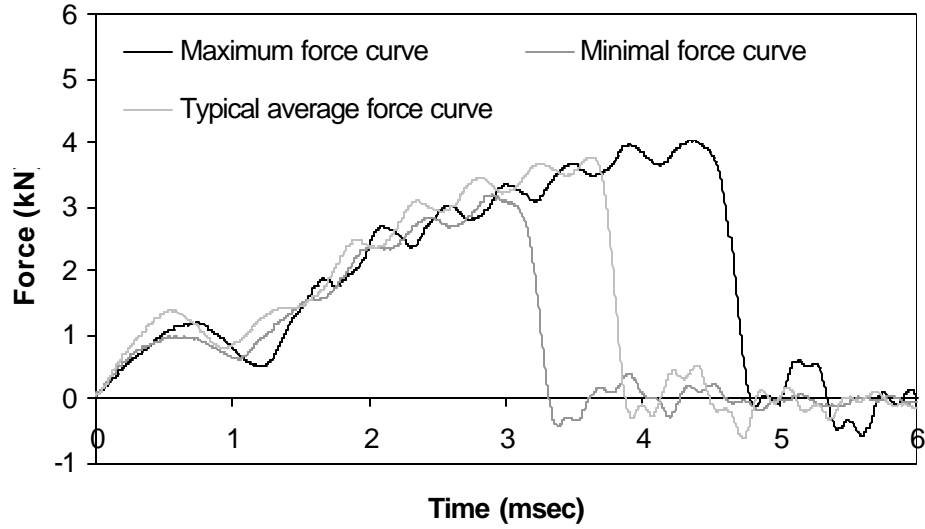


Figure 8. Force versus time for the laboratory tested wood specimens.

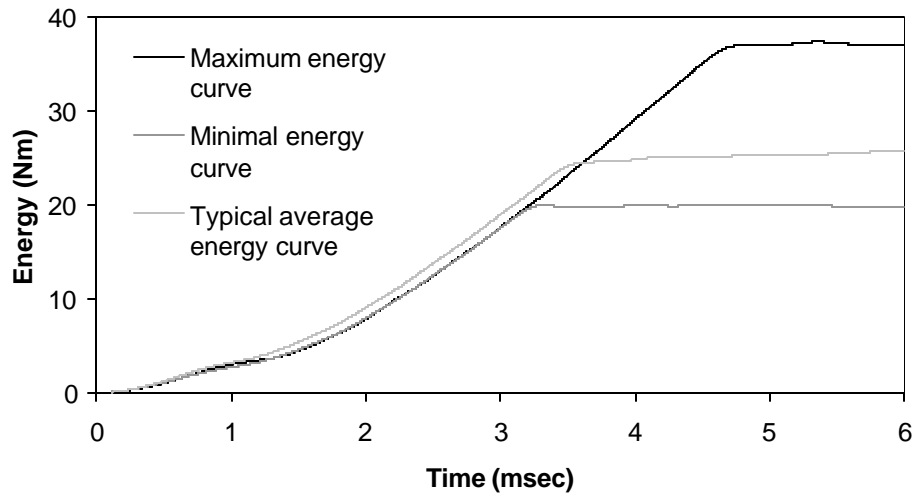


Figure 9. Energy versus time for the laboratory tested wood specimens.

The figures and the table above show that the results are relatively consistent even though the results vary for some of the results. The reason for the variation is probably that there were so many specimens so they all did not come from the same piece of wood and as discussed earlier wood properties change depending on environmental conditions and some pieces might also have defects like knots that affect the results.

4.2 FE Modeling

The material model used to model wood behavior in this research is material number 13, an isotropic material with a failure model. This material is not perfect for modeling wood but it is the best of the now existing material models in LS-DYNA. The properties used in the model are shown in Table 6. The choice of properties are based on earlier research performed in FE modeling of wood. (10)

Material type	13	Isotropic-elastic-plastic with failure
Element type	Solid	14-point integration
Density	610	Kg/m ³
Poisson's ratio	0.3	
Shear modulus	4231	Mpa
Bulk modulus	9167	Mpa
Yield stress	40	Mpa
Failure pressure	-49	Mpa

Table 6. Properties used in the FE model of wood specimen for validation of material model.

As can be seen in the table above, the failure pressure is changed from -90 MPa, the failure pressure used in the reference, to -49 MPa. This is to get the desired behavior of the modeled specimen, which is the behavior from the laboratory tests where the

specimen fails, which does not happen in the model if the failure pressure is lower than – 49 MPa.

The model is made as the laboratory setup with a wood specimen resting on two plates and is impacted by a cylinder that has the same mass and velocity as in the laboratory tests. A picture of the model is shown in Figure 10.

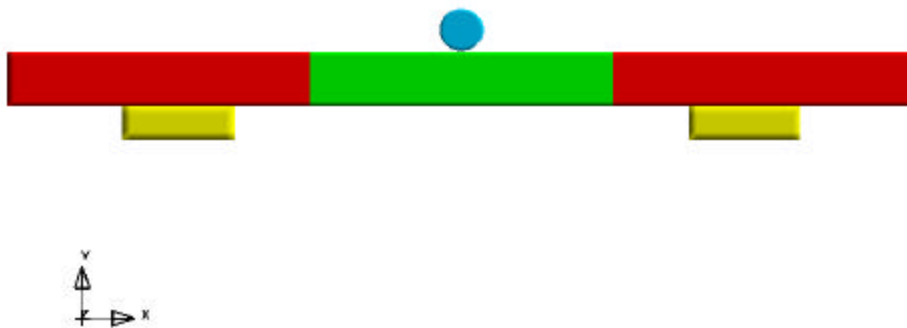


Figure 10. The model used in the validation of wood material model.

The simulation runtime statistics for the model above can be seen in Table 7.

Solid hexahedron elements	24023
Run time	4 hr 35 min
Hardware	IBM
No. of CPU	2
Processor speed	550
Simulated time	0.015 sec

Table 7. Simulation runtime statistics for wood material validation model.

Deflection time history for the model is shown in Figure 11.

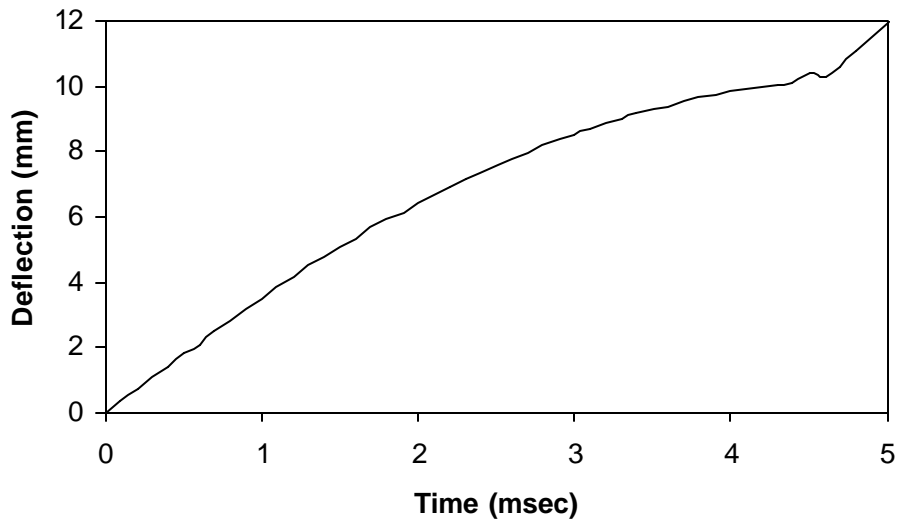


Figure 11. Deflection versus time for the model used in the material validation for wood.

The deflection at failure in the simulation is around 11 mm and failure occurred at time 5 msec. The force time history and the energy time history are shown in Figures 12 and 13.

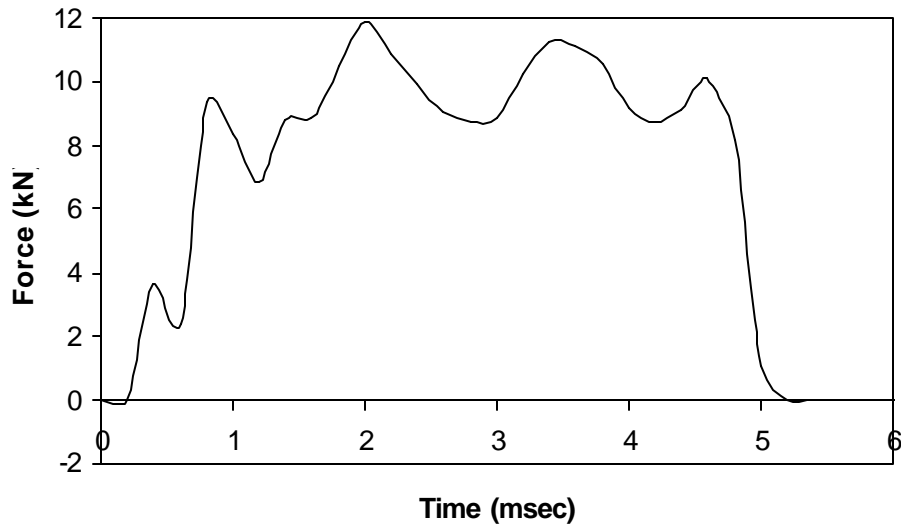


Figure 12. Force time history for the model used in the material model validation.

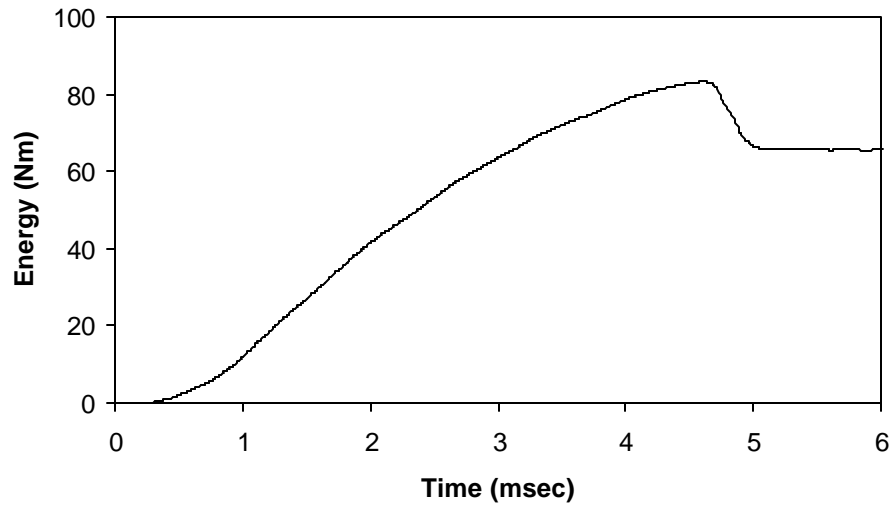


Figure 13. Internal energy time history for the model used in the material model validation.

4.3 Comparison and Validation

When the laboratory tests and the model were compared the results differed as shown in Figures 14, 15 and 16.

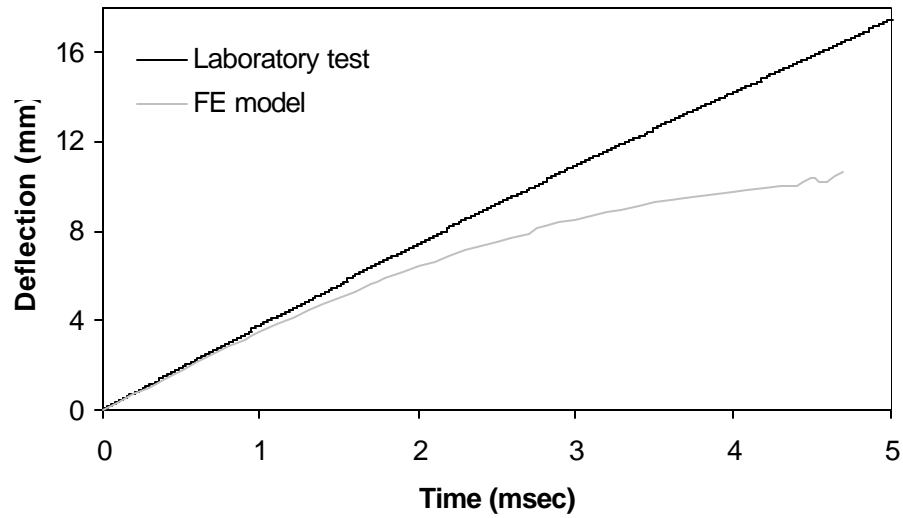


Figure 14. Deflection versus time comparison between laboratory test and FE model.

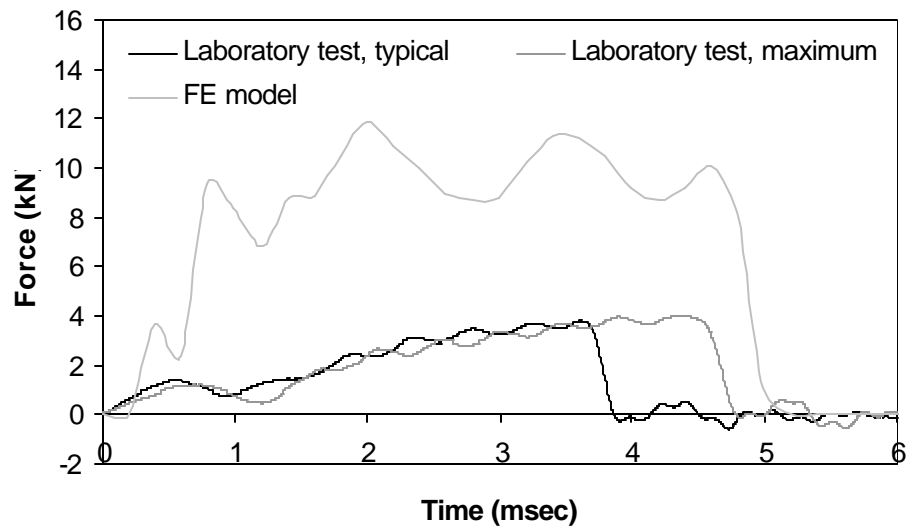


Figure 15. Force time history comparison between laboratory tests and FE model.

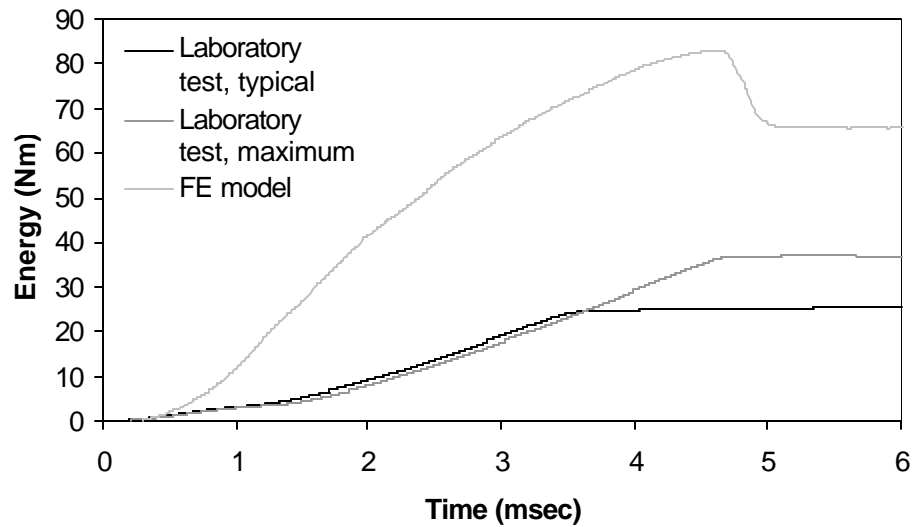


Figure 16. Energy time history comparison between laboratory tests and FE model.

The results between the laboratory tests and the FE simulation differ with a factor around 2 or 3, which can be seen in the figures above, except for the deflections, which agree best of the three compared results. For the laboratory tests, the maximum force is around 4 kN and for the model it is around 12 kN and the energies are 30 Nm and 70 Nm respectively. The reason for this difference is unfortunately not known at this point.

From the results above a conclusion of what a suitable material model for wood is can not be done. Because of this the earlier used material model from literature references with its properties will be used in the future research of this work when modeling wood material. (10)

5. SIMPLE ONE-POST SUB-MODEL

The reason for using a sub-model with only one post instead of a complete model of a guardrail system is to get an understanding of the behavior of a guardrail post within a reasonable runtime. A full FE simulation with a 30 meter guardrail and a vehicle is extensive and has much longer computation time.

The problem is decomposed into two events: lateral loading and wheel contact. The lateral loading shows how the post deflects in the soil and the wheel contact event shows whether the wheel snags on the post or not.

5.1 Lateral Loading

The first phase of the post deformation is the lateral displacement in the soil during the first part of the impact. At this point the vehicle is still upstream from the post and the post is responding to forces transmitted by the guardrail.

The first post that was modeled was a standard 150x200 mm grade 2 wood post. The post was modeled without a guardrail attached as shown in Figure 4. A standard impact scenario was developed to make the model comparable with the known test performance of the post. In the standard scenario the post is struck by a cylinder with a mass of 1400 kg and velocity 32 km/hr. The choice of mass and velocity is based on physical laboratory tests. The velocity of the cylinder is the same as in the test and the mass is approximately the same as in the test where the mass is 1390 kg. (15) The cylinder has a

length of 800 mm and a radius of 250 mm and is shown in Figure 17. The soil properties were changed so that the model displacement replicates the full-scale tests that had a maximum dynamic displacement in guardrail height that were 866 mm. (6) The post and soil properties that were used were validated by Plaxico *et al* (10) and are shown in Table 8. The failure pressure differs from earlier analysis since in full-scale tests the 150x200 mm wood posts do not tend to fail and the failure pressure is therefore increased noticeably compared to earlier used values.

Non-failing region:		
Material type	3	Isotropic-elastic-plastic
Element type	solid	1-point integration
Density	610	kg/m ³
Mod. of elasticity	11	GPa
Poisson's ratio	0.3	
Yield stress	40	MPa
Tangent modulus	11	MPa
Failure region:		
Material type	13	Isotropic-elastic-plastic with failure
Element type	solid	14-point integration
Density	610	kg/m ³
Poisson's ratio	0.3	
Shear modulus	4231	MPa
Bulk modulus	9167	MPa
Yield stress	40	MPa
Failure pressure	-1.0E+20	MPa
Internal angle of friction	45°	
Dry unit weight of soil	1.7752E-05	N/mm ³
Moisture content	0.08	

Table 8. Post and soil properties used in the model of the wood post.

STEP 02 TMC = 2.0249401E-01

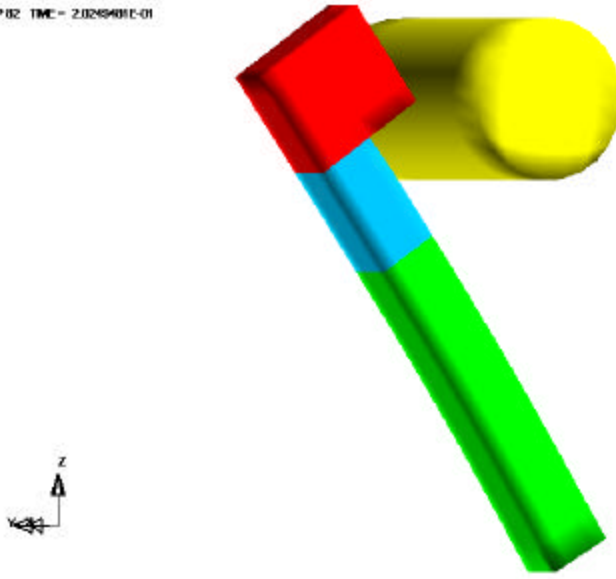


Figure 17. Standard 150x200 mm grade 2 wood post struck by a 1400 kg cylindrical impactor at 32 km/hr.

Simulation runtime statistics for the simulation can be seen in Table 9.

Solid hexahedron elements	632
Run time	50 min
Hardware	Pentium II
No. of CPU	1
Processor speed	450 MHz
Simulated time	0.40 sec

Table 9. Simulation statistics for the standard 150x200 mm wood post sub-model.

In the simulation of the 150x200 mm wood post a maximum dynamic deflection at guardrail height using the reference case were 866 mm. This result agrees well with full-scale tests performed with this kind of post, where the maximum deflection at guardrail height were 820 mm. (6)

The second post modeled was a W150x13.5 steel post. The material and soil properties used in this model are shown in Table 10.

Material type	24	Isotropic-elastic-plastic
Element type	Shell	Belytschko-Tsay integration
Density	7860	kg/m ³
Mod. of elasticity	200	Gpa
Poisson's ratio	0.3	
Yield stress	315	Mpa
Internal angle of friction	45°	
Dry unit weight of soil	1.7752E-05	N/mm ³
Moisture content	0.08	

Table 10. Properties used in the steel post model.

This post fails in lateral torsional buckling when struck by the cylinder in the reference case, see Figure 18. The same type of failure is observed in performed full-scale tests as shown in Figure 19. (6) This post was not used in the physical test series when the impact velocity was higher than 5.9 m/sec because lateral torsional buckling started to appear also in the tests. (14) Instead the W150x23.5 steel post was used for higher velocities in order to isolate the energy dissipation in the soil.

STEP 02 TMC = 2.900000E-01

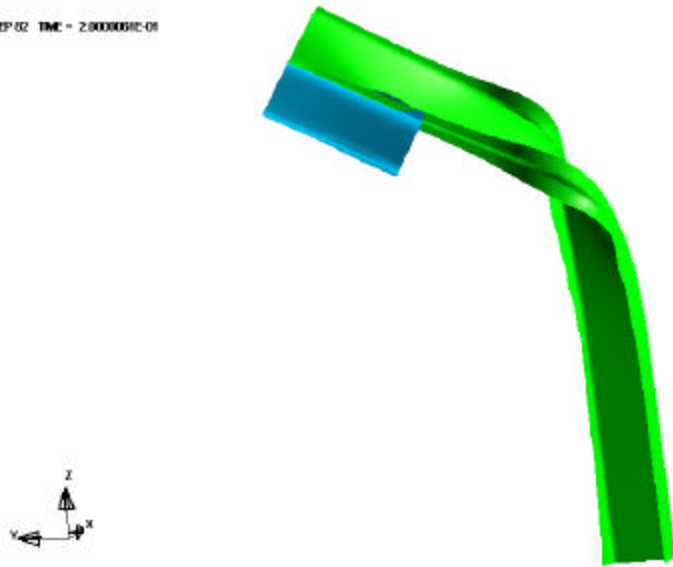


Figure 18. Maximum deflection of a steel W150x13.5 post showing a lateral torsional buckling failure.

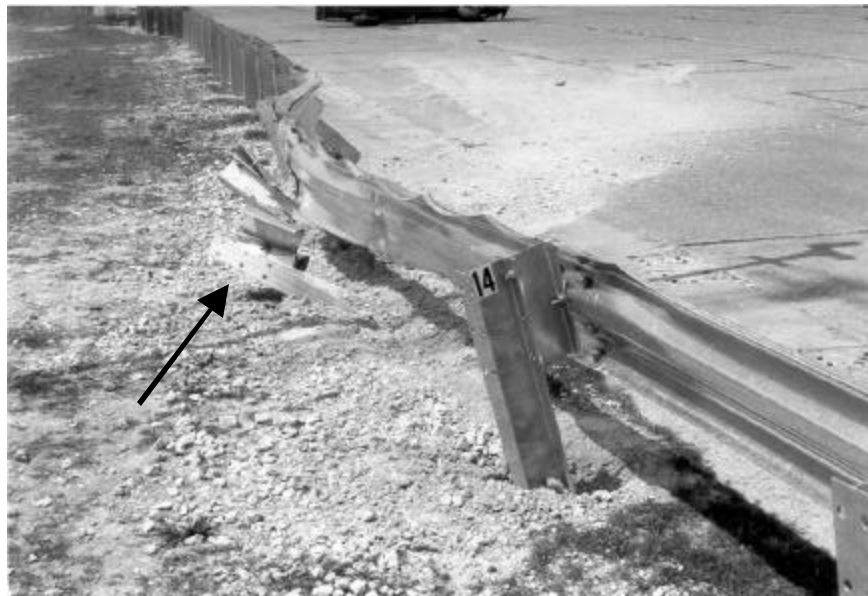


Figure 19. Deformation of a steel W150x13.5 post showing a lateral torsional buckling failure. (6)

The simulation runtime statistics for the steel W150x13.5 post are shown in Table 11.

Solid hexahedron elements	216
4-node shell elements	1456
Run time	40 min
Hardware	Pentium II
No. of CPU	1
Processor speed	450 MHz
Simulated time	0.40 sec

Table 11. Simulation statistics for the steel W150x13.5 mm and the steel W150x23.5 post sub-models.

The larger W150x23.5 steel post was investigated next and the same material properties as shown in Table 8 were used. The reference case conditions could be applied on this stronger post without initiating the lateral torsional buckling failure observed in the impact with the W150x13.5 as shown in Figure 20. This model had the same simulation statistics as the steel W150x13.5 post which are shown in Table 11.

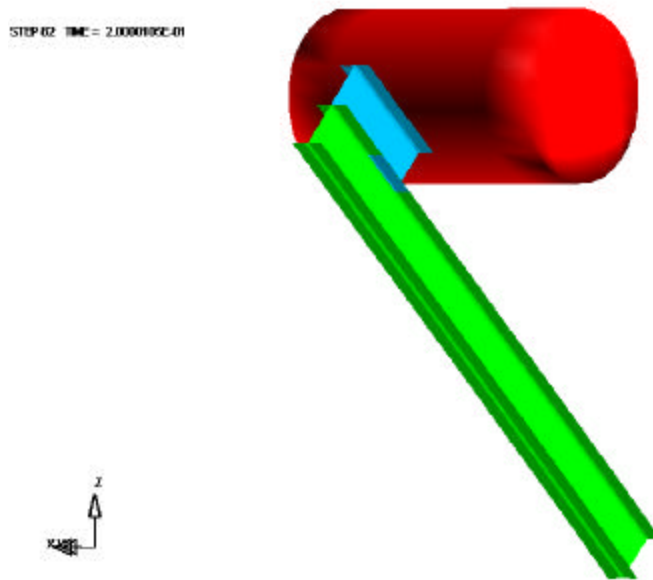


Figure 20. Steel W150x23.5 post struck by a 1400 kg cylindrical impactor at 32 km/hr.

The maximum dynamic deflection at guardrail height for the steel W150x23.5 post with the reference case applied is 1100 mm. This result can not be compared to a full-scale test since there are no tests performed on this type of steel post.

The force and energy time histories for the post bending simulations with the cylindrical striker for the different posts can be seen in Figures 21 and 22. Because of the average filter that is used in the force time history the curves do not start at origin since the first two points differ a lot in force but not in time and the filtering calculates the average values between the points.

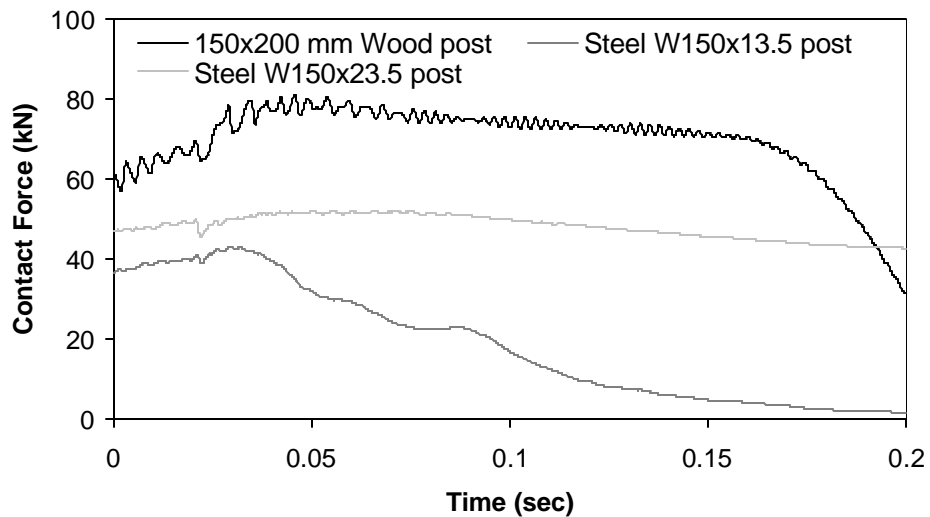


Figure 21. Force time history for the different posts bent by a cylindrical striker (100 point running average filter).

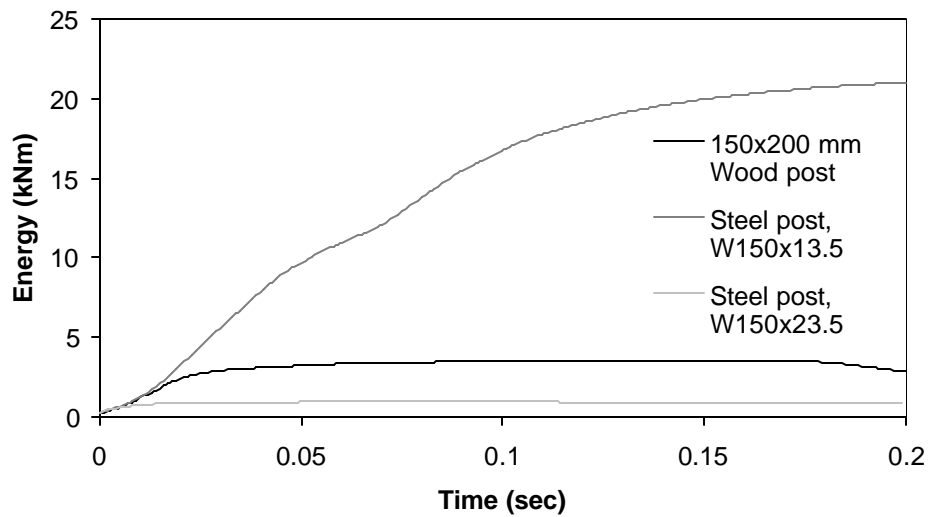


Figure 22. Post strain energy time history for the different posts bent by the cylindrical striker.

The maximum force required to bend the wood post (80 kN) is higher than for both steel posts (40 and 50 kN, respectively) as can be seen in Figure 21. The force for the W150x13.5 steel post is the lowest and that maximum force is around 40 kN. When the strain energies for the different posts are studied it can be seen that the steel W150x13.5 post has the highest strain energy which was expected since that post is bending and deforming much more than the other two posts. As expected the steel W150x23.5 deforms least and therefore has the lowest strain energy. The wood post does not bend or deform much either compared to the weaker steel post. The wood post and the W150x23.5 steel post behave like essentially rigid objects rotating in the soil. In impacts with the posts the soil can be expected to absorb the majority of the impact energy. The energy absorbed by the soil is the difference between the kinetic energy in the striker at the beginning of the event and the internal energy in the post plus the kinetic energy in the striker at each time as shown in the equation below.

$$U_{\text{soil},t} = \frac{1}{2}mv_0^2 - U_{\text{post},t} - K_{\text{striker},t}$$

where

m = impact mass,

$U_{\text{post},t}$ = strain energy absorbed by the post at time t ,

$U_{\text{soil},t}$ = strain energy absorbed by the soil at time t , and

$K_{\text{striker},t}$ = kinetic energy of the striker at time t .

The energy absorbed by the soil is shown in Figure 23.

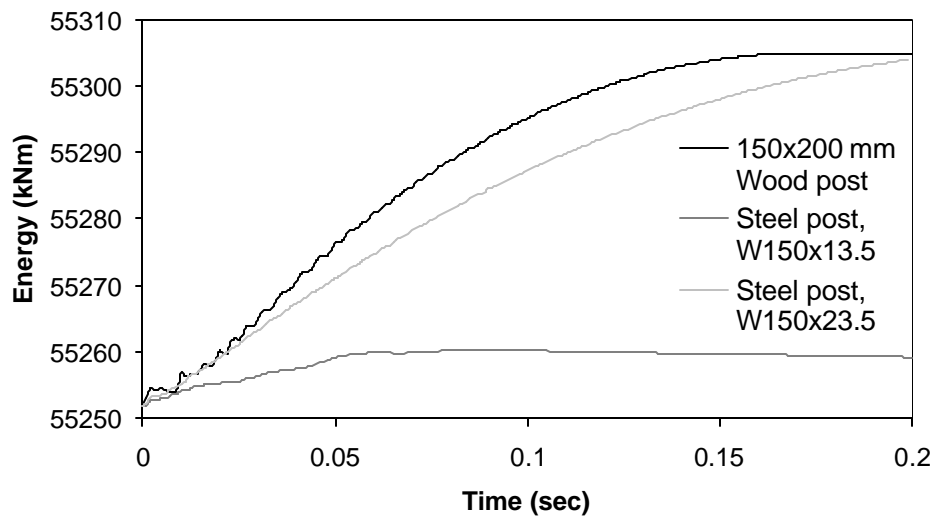


Figure 23. Energy absorbed by the soil for the different posts.

Figure 23 shows that the energy absorbed by the soil is least for the steel W150x13.5 post since this post deforms most and therefore absorbs most of the energy as strain energy.

For the other two posts, the energy absorbed by the soil is similar since the post behaves as an essentially rigid body.

The model showing the lateral loading of different posts is working satisfactorily at this point compared to the dynamic tests and the full-scale tests performed on those kinds of standard posts and the models can therefore be further developed.

5.2 Wheel-Post Contact

The second phase of post deformation occurs when the wheel of the impacting vehicle approaches the post. If the wheel can pass the post location without contacting it, the wheel will not snag on the post. If the wheel does contact the post, however, vehicle instability may result.

Once the post-soil models replicated the physical full-scale tests, a wheel from a pickup truck model with velocity 100 km/hr was assembled with the post-cylinder models to show snagging of the wheel on the post. The edge of the wheel was positioned at the same y-coordinate as the lower edge of the block-out as shown in Figure 24. The lower edge of the block-out represents the location of the guardrail. During a collision it is the guardrail that the vehicle would be in contact with.

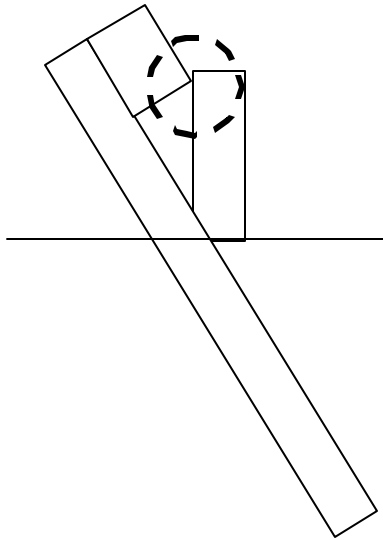


Figure 24. Sketch showing how the wheel is positioned related to the post.

Originally the wheel was constrained not to rotate or steer in x, y and z directions. The resulting behavior of the wheel after it hit the post was not realistic since it could not steer toward the post as could be the case in a real impact, however, this behavior is good enough for now since snagging can be shown anyway and is correct until after the wheel have struck the post. How the wheel snags on the standard 150x200 mm wood post can be seen in Figure 25.

STEP 02 TIME = 2.004807E-01

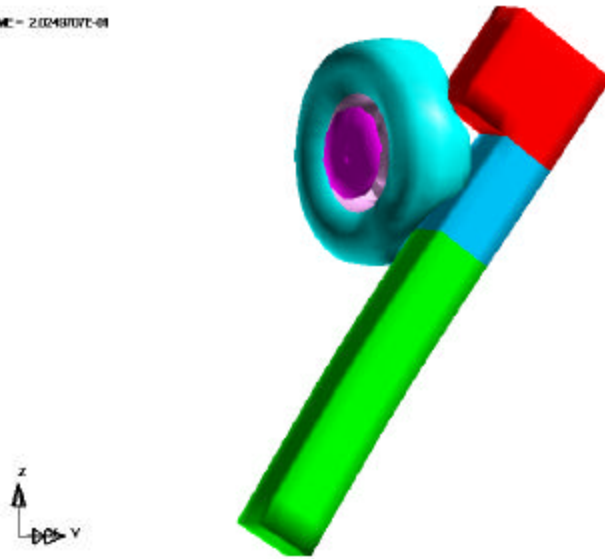


Figure 25. Wheel snagging on standard 150x200 mm grade 2 wood post.

Simulation runtime statistics for the model above can be seen in Table 12.

Solid hexahedron elements	678
Beam elements	4
4-node shell elements	570
Run time	60 min
Hardware	Pentium II
No. of CPU	1
Processor speed	450 MHz
Simulated time	0.40 sec

Table 12. Simulation statistics for the standard 150x200 mm wood post sub-model with wheel contact.

When the model worked with the lateral load (the cylinder) for both of the steel posts, a wheel was introduced in the models the same way as for the wood post to simulate snagging. For the smaller W150x13.5 steel post the wheel runs over the post as it lies on

the ground as shown in Figure 26. The wheel snags on the larger W150x23.5 steel post as shown in Figure 27.

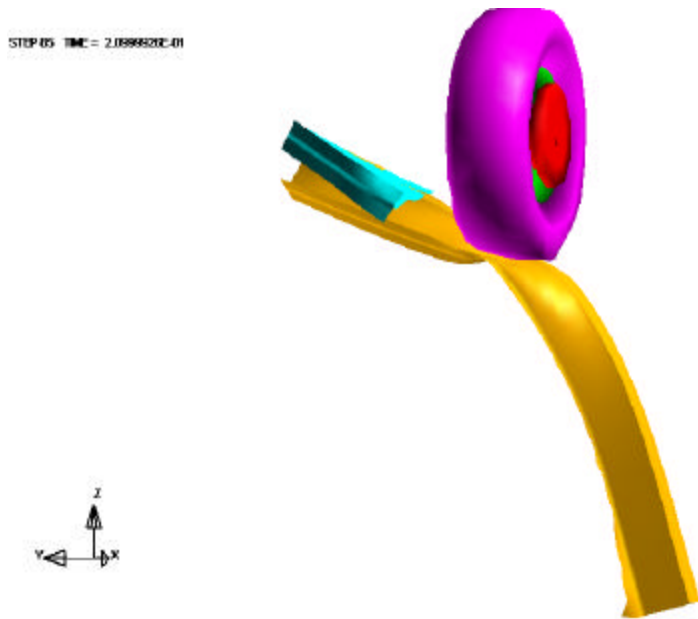


Figure 26. Steel W150x13.5 post and wheel.

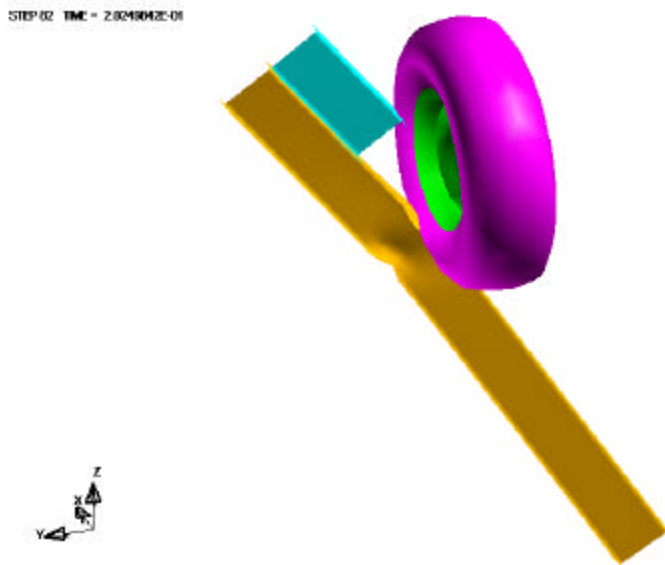


Figure 27. Steel post W150x23.5 and wheel that snag.

The simulation runtime statistics for the both steel posts is the same and are shown in Table 13.

Solid hexahedron elements	262
Beam elements	4
4-node shell elements	2026
Run time	120 min
Hardware	Pentium II
No. of CPU	1
Processor speed	450 MHz
Simulated time	0.40 sec

Table 13. Simulation statistics for steel posts, W150x13.5 and W150x23.5 post sub-models with wheel.

Those models that exhibit snagging of the wheel are realistic and adequate in describing when and how it happens but they are not correct after the collision since the wheel is restricted in its movement and can not steer in any direction. Since the goal with these models was to show that snagging occurs on existing standard posts and not how the wheel behaves after it struck the post, the models are working adequately for this purpose. Later on a development of the wheel model is necessary to be able to notice for example changes in forces for different alternatives. According to full-scale tests that have been performed the wheel snags on those types of existing standard posts, which is also the occurrence in the simulations where the wheel is assembled in the sub-models.

(3)(4)(5)(6)(7)(8)

While the models above still do not show a realistic behavior of the wheel after it strikes the post, they do show the conditions that cause wheel snagging. To make the model more realistic and allow the wheel to steer, the wheel was attached to a 2000 kg block

which had the same inertial properties as a 2000 kg pick-up truck. This improvement in the model is necessary since the correct behavior of the wheel after the collision will increase or decrease the degree of snagging. The suspension was modeled with a joint and a spring. This might over predict the suspension forces compared to a real case since the joint in the model is rigid and not able to deform and therefore exhibit a stiffer behavior. In the model without the block attached to the wheel, the wheel could not steer at all, which was not realistic. Also the contact between the wheel and the block-out were removed so it is possible to study the snagging of the wheel on the post without any interaction and contact between wheel and block-out.

The model of the standard 150x200 mm wood post was the first one developed with the wheel with the vehicle inertia included as shown in Figure 28.

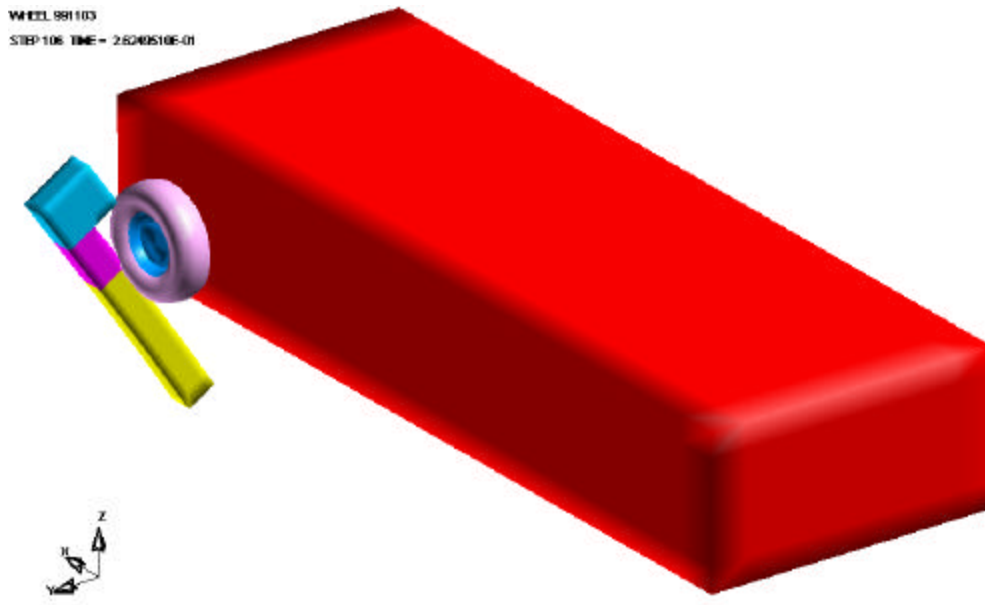


Figure 28. The model with the wheel attached to a block.

Simulation runtime statistics for the model are shown in Table 14.

Solid hexahedron elements	1638
Beam elements	4
4-node shell elements	570
Run time	40 min
Hardware	Pentium II
No. of CPU	1
Processor speed	450 MHz
Simulated time	0.40 sec

Table 14. Simulation statistics for wood post sub-model with wheel attached to a block.

This wheel with vehicle inertia was also assembled with the model of the steel W150x13.5 post as can be seen in Figure 29.

WHEEL SUB-MODEL
STEP 118 TIME = 2.924088E-01



Figure 29. The steel W150x13.5 post assembled with the wheel with vehicle inertia.

Simulation runtime statistics for the run with the steel W150x13.5 post is shown in Table 15.

Solid hexahedron elements	1222
Beam elements	4
4-node shell elements	2026
Run time	2 hr 55 min
Hardware	Pentium II
No. of CPU	1
Processor speed	450 MHz
Simulated time	0.40 sec

Table 15. Simulation statistics for steel W150x13.5 post sub-model with wheel attached to a block

For the two models above with the wheel with the vehicle inertia included the resultant joint forces for the wheel and also the impulse delivered to the wheel can be seen in Figures 30 and 31. The impulse curves correspond to the area under the joint force curves.

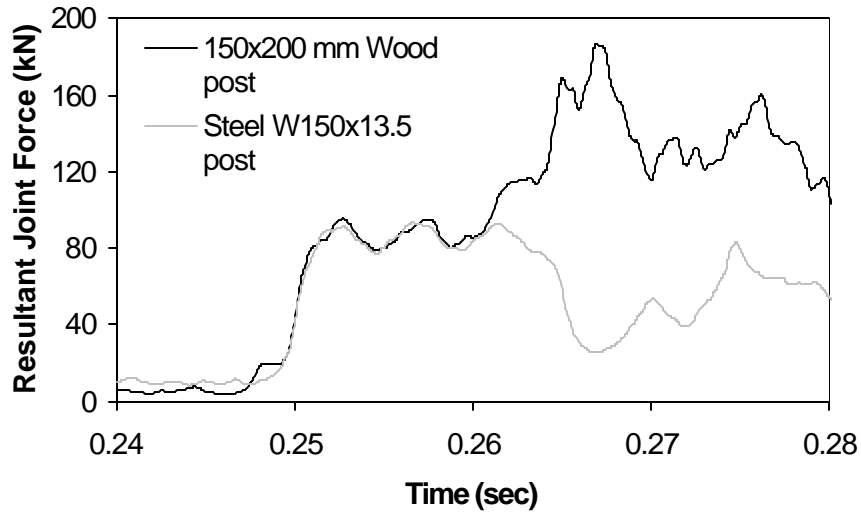


Figure 30. Resultant joint force versus time for 150x200 mm wood post and steel W150x13.5 post (filtered to SAE 60).

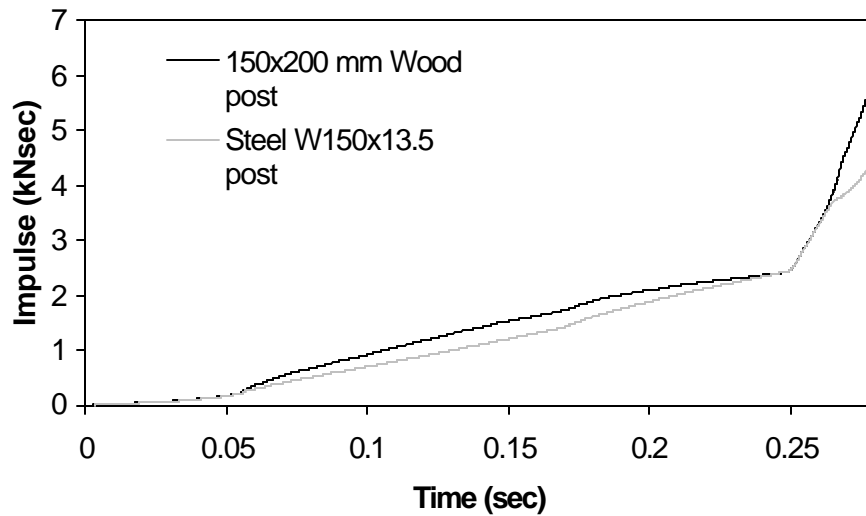


Figure 31. The impulse delivered to the wheel for the 150x200 mm wood post and the steel W150x13.5 post.

The figures above show that the maximum joint force is higher for the wood post than for the steel post as expected, 180 kN and 100 kN respectively, since the steel post deforms to an almost horizontal position as can be seen in Figure 29. Since the post is collapsed on the ground it is easy for the wheel to pass over the post without any severe interaction. The same can be seen when studying the impulse diagram where the impulse delivered to the wheel is less for the steel W150x13.5 post for the same reason and is around 4 kN-sec compared to 6 kN-sec for the wood post.

A test of a wood post W-beam guardrail results in the wheel being torn off the vehicle whereas a similar test with a steel post does not. (6) This information combine with Figures 30 and 31 suggest that, a joint force over 100 kN, which corresponds to a impulse of approximately 6 kN-sec, is required to tear off a wheel from a vehicle that is exposed

to wheel snagging can be done. This conclusion can be made since 150x200 mm wood posts with 190 mm block-out depth causes this type of occurrence according to full-scale tests performed. (6) The steel W150x13.5 post that performs this behavior as shown above has in full-scale tests caused vehicle rollover.

A model with the wheel with vehicle inertia is not developed for the steel W150x23.5 posts since the behavior of that type of post is similar to the standard 150x200 mm wood post and another reason is that this post is not often used in reality.

6. POST ALTERNATIVES

There are a variety of methods that could be used to reduce the potential for wheel snagging:

- Deeper block-outs
- Longitudinal failure fuses
- Lateral failure fuses
- Different cross-sections

The two last alternative deals with lateral failure fuses and different cross-sections and are not included in this research and can be considered as suitable future work.

6.1 Deeper Block-outs

A potential method to avoid wheel snagging is to increase the block-out depth on a standard wood post as shown in Figure 32. This design will increase the distance between the wheel and the post and that will decrease the forces and accelerations on the wheel.

When the block-out is deep enough to prevent contact between the wheel and the post, no snagging will occur.

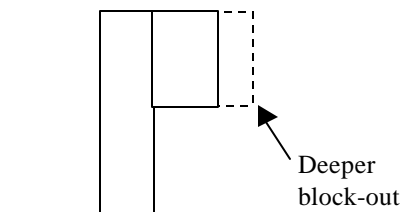


Figure 32. Sketch showing deeper block-out.

6.2 Longitudinal Failure Fuses

Another alternative is to investigate if a breakaway mechanism such as holes in the longitudinal direction through a wood post would prevent snagging by allowing the wheel to break the post if there is direct contact between the wheel and the post, see Figure 33. The holes make the post weaker and when the forces between the post and the wheel reach a critical value the post fails instead of snagging the wheel. The investigation should start with the existing CRT post and then make different changes to develop a new design that will improve the properties that prevent snagging.

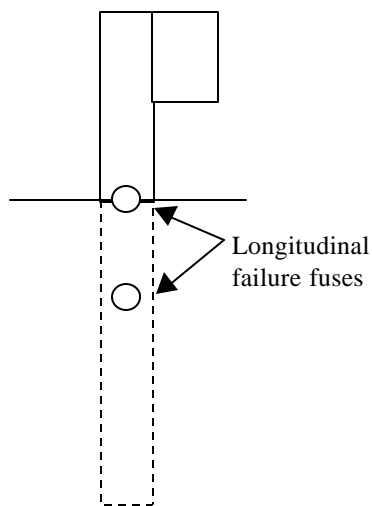


Figure 33. Sketch showing post with longitudinal failure fuses.

6.3 Lateral Failure Fuses

The same solution as for the longitudinal failure fuses but here the fuses will be in the lateral direction instead of the longitudinal, see Figure 34. When the post rotation reaches a point where snagging would occur, the post is designed to fail allowing the wheel to pass by without interacting with the post.

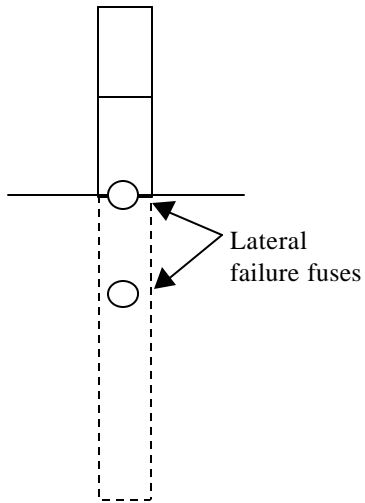


Figure 34. Sketch showing post with lateral failure fuses.

6.4 Different Cross-sections

The third alternative is to redesign the steel post by using another cross-section than the standard I-shape or rectangle shape. Those cross-sections can be square or circular but should have the same moment of inertia as the original steel post. One more thing to do with these new shape posts is to try another material, like high-density polyethylene.

Another alternative is a x-post made of steel with a tube block-out.

7. FINITE ELEMENT ANALYSIS OF ALTERNATIVES

7.1 Deeper Block-outs

This alternative involves increasing of the block-out depth on a standard 150x200 mm wood post until snagging is reduced or prevented. Reducing the overlap between the wheel and the post reduces snagging. If there is no overlap at all no snagging should occur. Overlap is defined in Figure 35.

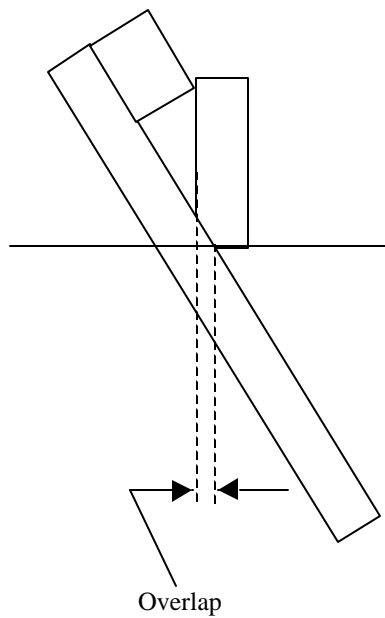


Figure 35. Definition of overlap.

A FE model of the wood post with different block-out depths was developed. The wood post were modeled without failure, which coincide with the full scale testing that has been performed where the wood post does not fail at collision. (6) The standard wood strong post guardrail uses a 190 mm deep block-out. The block-out depth was increased by increments of 10 or 20 mm to a maximum block-out depth of 250 mm. At that depth

there was no snagging of the wheel as shown in Figure 36. For all block-out depths smaller than 250 mm, snagging occurred. Figure 37 shows how the overlap between the wheel and the modeled wood post varies with the block-out depth.

STEP 106 TIME = 2.6248830E-01

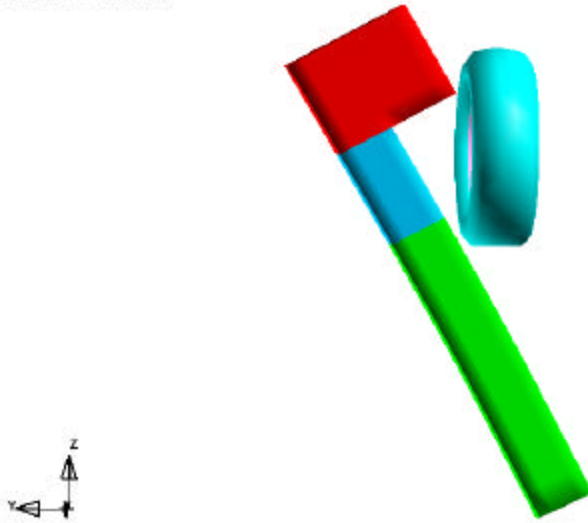


Figure 36. Wood post with block-out depth 250 mm, which prevent wheel from snagging.

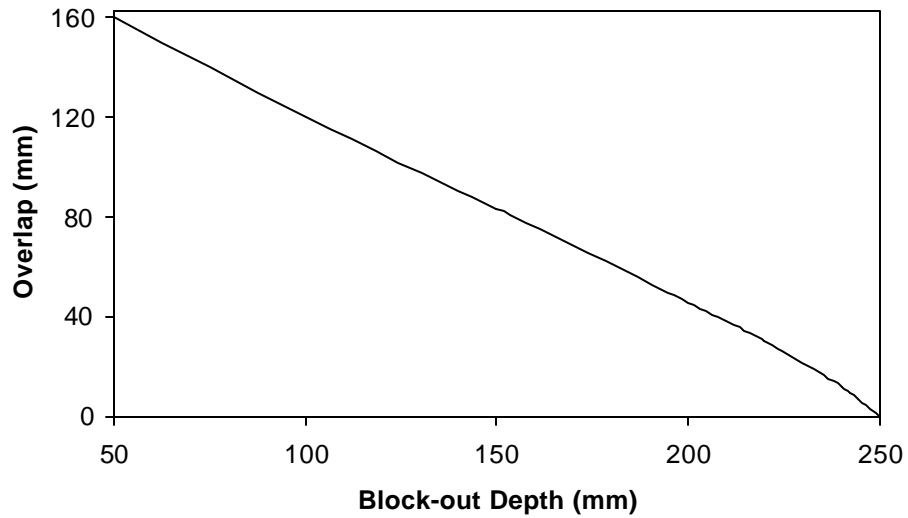


Figure 37. The overlap variation against the block-out depth for wood post.

For the standard 150x200 wood post a block-out depth of 250 mm is required to completely prevent snagging and reduce the overlap to zero as can be seen in the figure above.

The resultant joint forces for the wheel were measured in the simulation and, as shown in Figures 38 and 39, the forces decrease with increasing block-out depth. Reducing the amount of overlap therefore decreases the forces experienced by the wheel and therefore the severity of the snagging event also reduces.

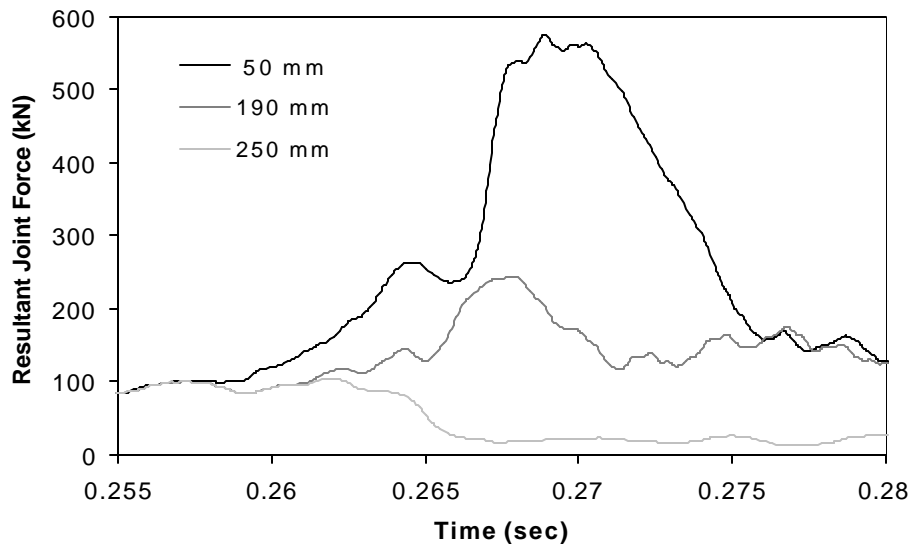


Figure 38. Resultant joint force versus time for different block-out depths (filtered to SAE 60).

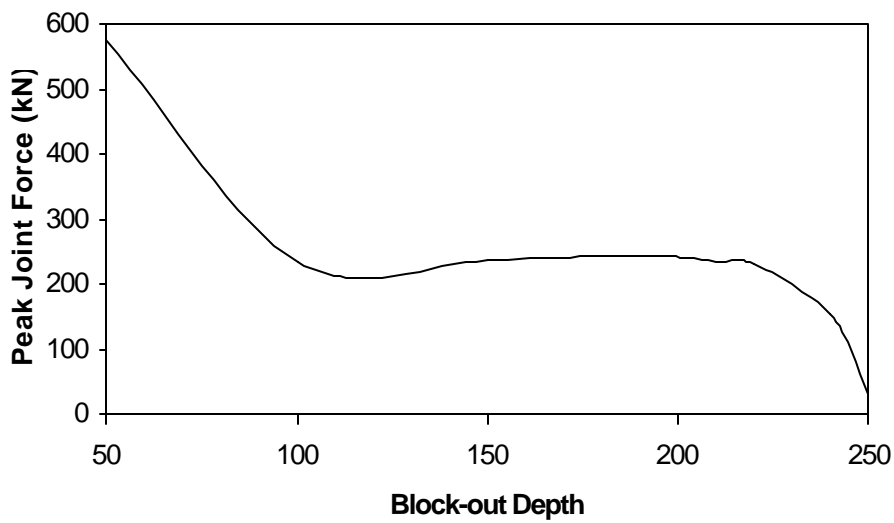


Figure 39. Resultant peak joint force variation for different block-out depths.

Figures 38 and 39 show that the joint force decreases with increasing block-out depth. As the block-out becomes deeper, the overlap decreases and this reduces the interaction forces between the wheel and the post. The impulse delivered to the wheel is the area

under each curve in Figure 38. As the block-out depth is increased, the impulse transmitted to the wheel is decreased. This decrease in force and impulse should correspond to less vehicle instability. It is interesting to note that the peak joint force is nearly the same for block-outs between 100 and 200 mm deep. In order for a deeper block-out to be effective in reducing the impulse, the block-out must be at least 60 mm deeper than the standard 190 mm deep block-out. In full-scale tests a block-out depth of 190 mm is not enough to prevent a wheel from snagging and for this block-out depth the joint force is around 250 kN. (6) This means that a force of that size on the wheel is enough for the wheel to tear off or make the vehicle roll over since this has been observed in full-scale crash tests.

While the models above do not show a realistic behavior of the wheel after it strikes the post as discussed earlier, they do show the required block-out depth to prevent snagging. To study a more realistic behavior of the wheel the model of the wheel with vehicle inertia was assembled with the post models with the different block-out depths. The simulation runtime statistics is the same as before for the 150x200 wood post which are shown in Table 12. In this model the same maximum block-out depth of 250 mm that is required to prevent snagging is used as in the earlier model. The joint forces for the wheel in this case differ from the earlier case and can be seen in Figure 40. The impulse delivered to the wheel for the different block-out depths can be seen in Figure 41. The impulse curves correspond to the area under the joint force curves. The wheel hits the

post around the time 0.260 seconds and the contact ends around 0.280 seconds as can be seen in the figures below.

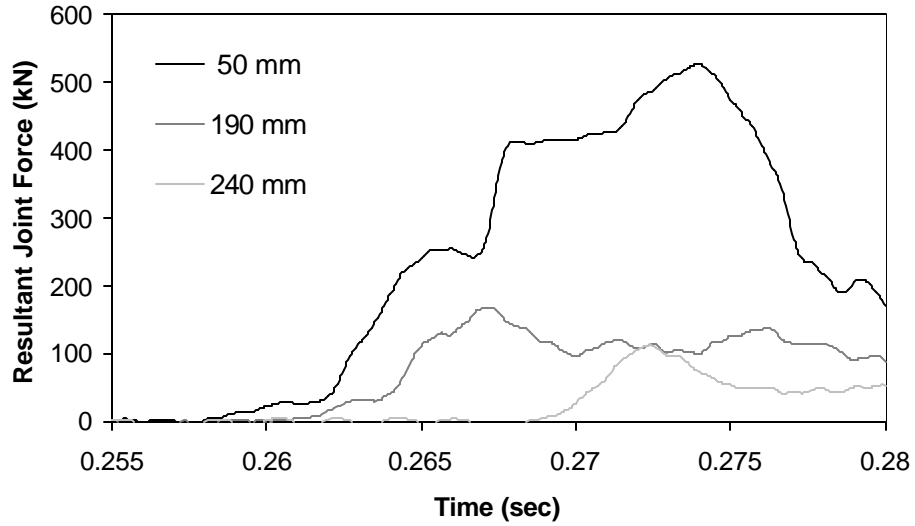


Figure 40. The resultant joint force curves subtracted by the joint force curve for the block-out depth 250 mm (filter to SAE 60).

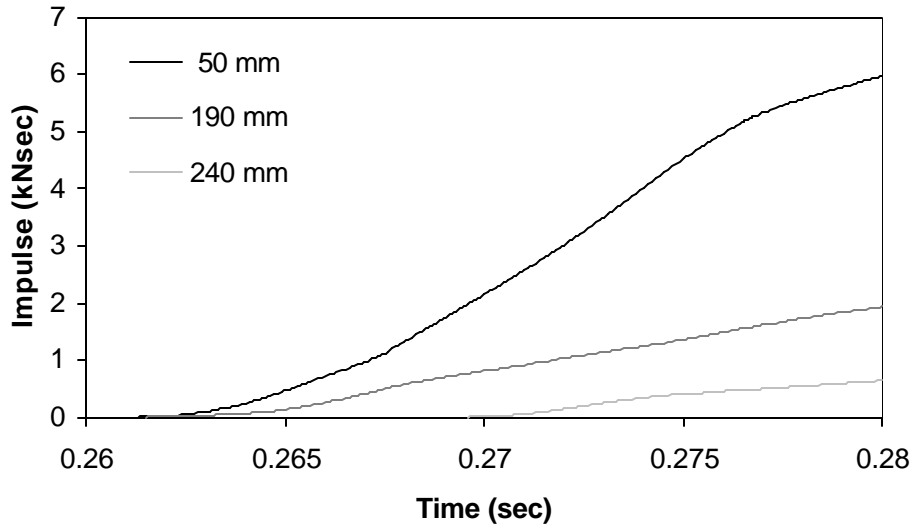


Figure 41. The impulse delivered to the wheel at the different block-out depths after the 250-mm block-out depth curve is subtracted.

Figures 40 and 41 show that the joint forces and the impulses decrease with increasing block-out depth as expected and as shown for the previous model. The joint forces in the case with vehicle inertia included are similar to the case without vehicle inertia but it gives more realistic results since the wheel can steer. Those results show the same trend as the ones given earlier that as the block-out becomes deeper, the overlap decreases which reduces the interaction forces between the wheel and the post. From this it also follows that the impulse delivered to the wheel decrease with increasing block-out depth since the impulse corresponds to the area under the force displacement curve for each block-out depth. Since the resultant joint forces for the block-out depth that prevents snagging (250 mm) should be zero or negligible, the curves for the other block-out depths are subtracted with the values from the original curve which is done in Figure 40. The same for the impulse curve where the impulse delivered to the wheel should be zero for

the non-snagging block-out, and is therefore subtracted from the other impulse curves, see Figure 41. The reason for those curves, that correspond to the block-out depth that prevent snagging, not being zero is that there are other factors that contribute to the forces on the wheel such as its own acceleration and rotation.

The variation of the impulse delivered to the wheel right after the contact between wheel and post have ended, which is around 0.28 seconds, for the different block-out depths are shown in Figure 42.

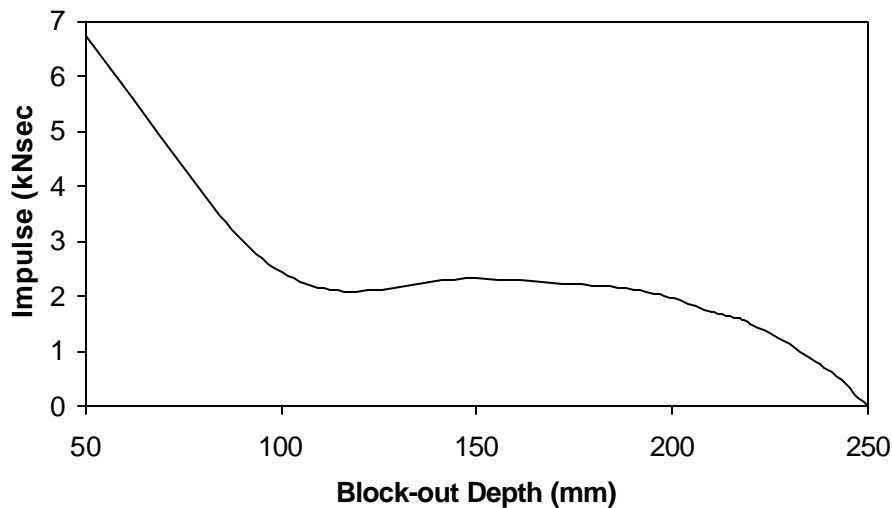


Figure 42. The block-out depth versus the impulse delivered to the wheel.

Figure 42 shows the same trend as for the earlier case without the vehicle inertia included. The trend shown is that in order for a deeper block-out to be effective in reducing the impulse between the wheel and the post, the block-out depth must be increased at least 60 mm compared to the standard 190 mm deep block-out for a total minimum block-out depth of 250 mm. According to the full-scale crash tests that have

been done with the standard wood post with a block-out depth of 190 mm, the tire on the impact-side of the vehicle hits the post and shortly thereafter, the wheel assembly separated from the vehicle. (6) (12) As can be seen in the figures above, it requires a joint force around 180 kN and an impulse of 2 kN-sec to tear off the wheel from the vehicle when a standard 190 mm deep block-out is used. The impulse was 6 kN-sec before the non-snagging post impulse curve was subtracted as can be seen from earlier results for the standard 150x200 mm wood post. This could be prevented if the block-out depth is increased and according to the results above the depth should be increased to at least 250 mm. Any increase of the block-out depth reduces the forces on the wheel as can be seen in the figures above but there are no full-scale tests done on any other block-out depths than 190 mm so it is not possible to validate these results with physical experiments at this time.

All models developed above are modeled without failure but in reality wood can fail even though the wood post in the full scale tests performed for a block-out depth of 190 mm do normally not fail. For the block-outs less deep than 190 mm failure could be a possibility since the interaction between the post and the wheel increase. Figure 43 compares the joint forces on the wheel between a post with a 50 mm block-out depth modeled without failure and with failure. The failure pressure used in the model that allows failure is -90 MPa.

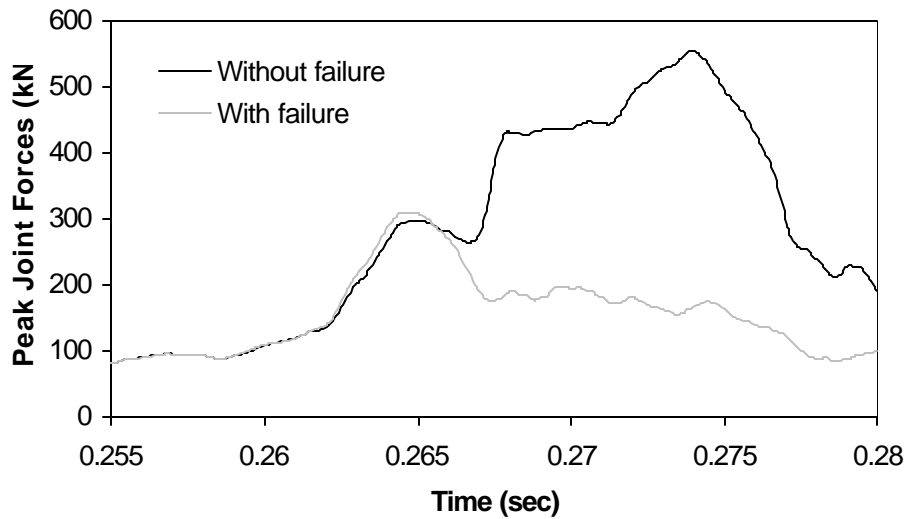


Figure 43. Comparison between resultant joint forces on the wheel for wood post modeled with and without failure for a block-out depth of 50 mm (filtered to SAE 60).

In the figure it can be seen that for the post modeled without failure, the joint force continues to increase after the wheel has contacted the post. For the post modeled with failure the force decrease and starts to plane out after collision as expected since the post failure allows the post to fracture and the wheel to pass by without further interaction with the post.

7.2 Longitudinal Failure Fuses

The next alternative is to investigate if a longitudinal breakaway mechanism on a wood post will prevent snagging. The breakaway mechanism functions like a fuse by causing the post to fail once a specific load is attained. The first model developed is of the existing CRT (Controlled Releasing Terminal) timber post, which is a post used in guardrail terminal installations. This post has two circular holes, one with its center at the

ground line and one 400 mm below the ground line, with a diameter of 90 mm as shown in Figure 44. The holes are drilled parallel to the direction of travel and are intended to weaken the post in the longitudinal direction while not appreciably affecting the lateral strength.

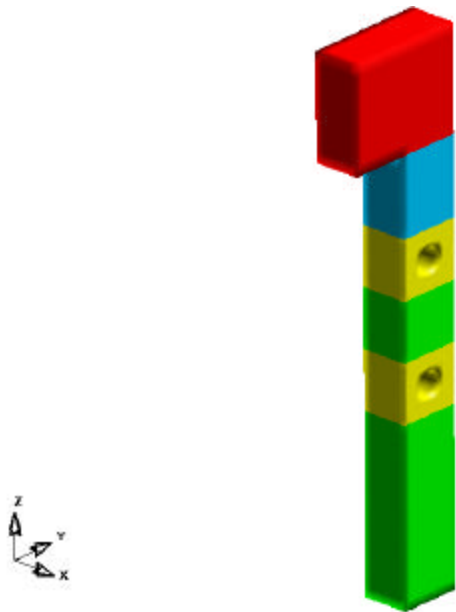


Figure 44. Model of the CRT timber post.

As a comparison between the standard wood and steel posts as well as the CRT post, Table 16 shows the mass moment of inertia for the two different posts. The coordinate system used can be seen in Figure 45.

Type of Post	I_{xx} (mm ⁴)	I_{yy} (mm ⁴)
150x200 mm wood post	80.0×10^6	43.4×10^6
CRT wood post	71.5×10^6	22.9×10^6
Percent reduction	11 %	47 %

Table 16. The calculated mass moment of inertia for standard wood post and CRT post.

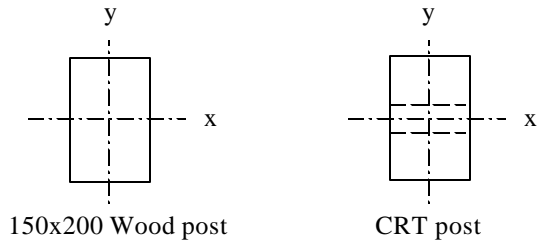


Figure 45. Sketch showing coordinate system used in calculations of mass moment of inertia.

The mass moment of inertia for the 150x200 mm wood post should be similar to the CRT post in the x direction and differ more in the y direction. In the table it can be seen that the mass moment of inertia for the standard wood post is very similar in x direction and about 2 times higher in y direction than the CRT post as expected. As shown in Table 16 the CRT post is nearly 50 percent weaker in the longitudinal direction while it is only 11 percent weaker in the lateral direction. A wheel striking the CRT post should be able to break the post easier than a standard 150x200 wood post.

The properties used in this model is the same as for the standard 150x200 mm wood post, see Table 6, except for the failure pressure that is -90.0 MPa at the two sections section with the holes in this case since failure of the post is desired. The element density is higher where the holes are located than on the rest of the post. The element type at these two sections is 14-point integrated element instead of the default solid elements with constant stress. Also the section in between the holes and the lower section have 14-point integrated elements but those parts of the post are not modeled with failure.

The modeled post is exposed to the standard case with the same conditions as before with a 1400 kg cylindrical impactor that strikes the post at a speed of 32 km/hr.

Simulation runtime statistics for the modeled CRT post is shown in Table 17.

Solid hexahedron elements	5442
Run time	23 hr 35 minutes
Hardware	IBM
No. of CPU	2
Processor speed	550
Simulated time	0.30 sec

Table 17. Simulation statistics for the modeled CRT post exposed to lateral loading.

This type of post fails at the lower hole because the stresses are highest at the lower hole in the lateral loading case as can be seen in Figure 46.

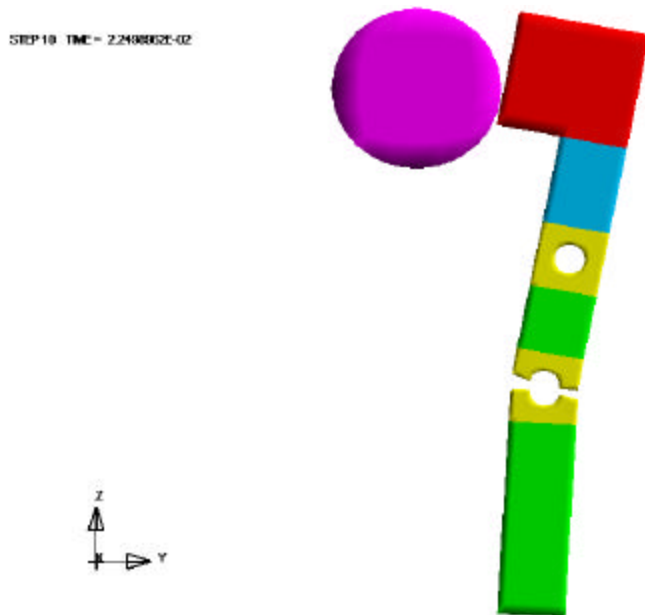


Figure 46. CRT post failure caused by lateral loading.

The post fails at a ground deflection around 100 mm and time 0.023 seconds. The deflection time history until failure is shown in Figure 47. This deflection is much less than for the ground line deflection for the standard post which is almost 500 mm.

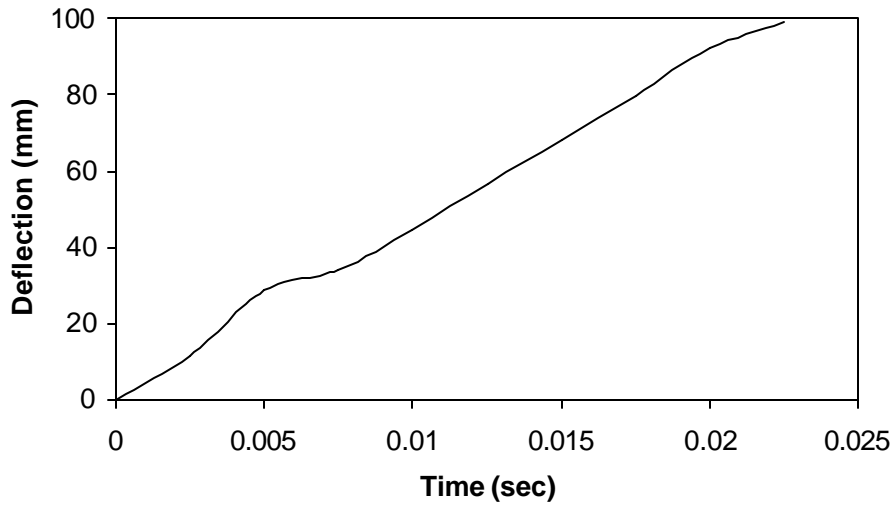


Figure 47. Deflection time history for the CRT post.

The contact force time history and the strain energy time history for the CRT post compared to the standard 150x200 mm wood post are shown in Figures 48 and 49.

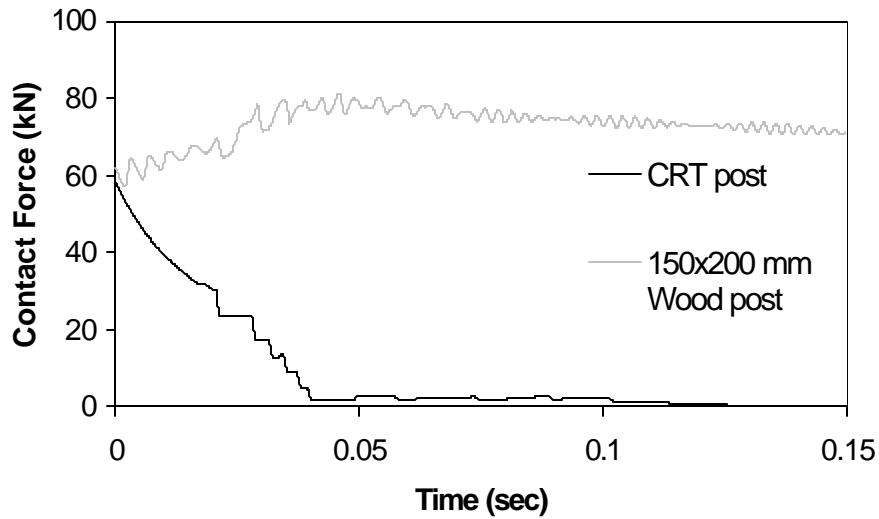


Figure 48. Force time history for the CRT post and for the standard wood post as comparison (100 point running average filter).

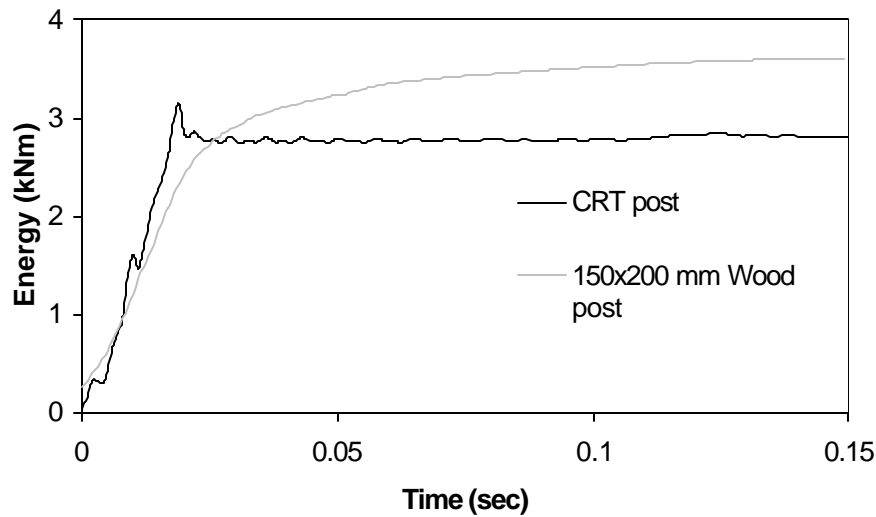


Figure 49. Post strain energy time history for the CRT post and for the 150x200 mm wood post as comparison.

In the figures above it can be seen that the CRT post fails around the time 0.023 seconds since the force curve make a sudden shape change from a smooth shape to a less smooth one since the forces becomes more uncontrolled after the failure. The energy curve for the CRT post shows an increasing curve similar to the one for the standard wood post until the post fails and at the same time the energy drops and then becomes constant.

Since the CRT post fails only by lateral loading there is no risk of wheel snagging on this type of post. If, for some reason, the wheel contacts the post without any lateral loading, the post would fail anyway as can be seen in Figure 50 where the model of the wheel with the vehicle inertia is included in the model of the CRT post. In this model the stone wall that is included in the wheel model acting as the ground line is removed and is replaced with a shell plate that acts as ground. The reason for this substitution is that

since the stone wall was located in the same height as the upper hole it was interacting with the failure mechanism of the post and made it fail at the upper hole after failure already occurred at the lower hole which does not seem realistic. This ground plate is not in contact with the post and is therefore not interacting with the post during failure as desired. The shell plate can also be seen in Figure 50. As can be seen in the figure the post fails at the lower hole, and the wheel is able to pass the post without severe snagging.

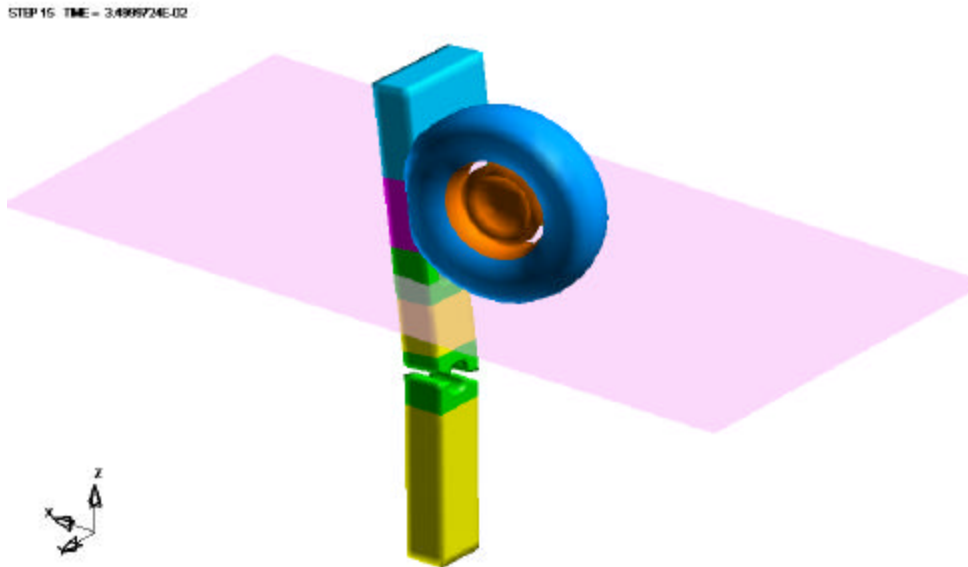


Figure 50. CRT post failure caused by wheel impact.

Simulation runtime statistics for the model above are shown in Table 18.

Solid hexahedron elements	6232
Beam elements	4
4-node shell elements	5421
Run time	8 hr 50 min
Hardware	IBM
No. of CPU	2
Processor speed	550
Simulated time	0.10 sec

Table 18. Simulation runtime statistics for the CRT post exposed to wheel contact.

The resultant joint forces on the wheel and the impulse delivered to the wheel for the model above are shown in Figures 51 and 52. The contact starts at 0.008 seconds and ends at 0.09 seconds and failure of the post occur at 0.035 seconds, which can also be seen in Figures 51 and 52.

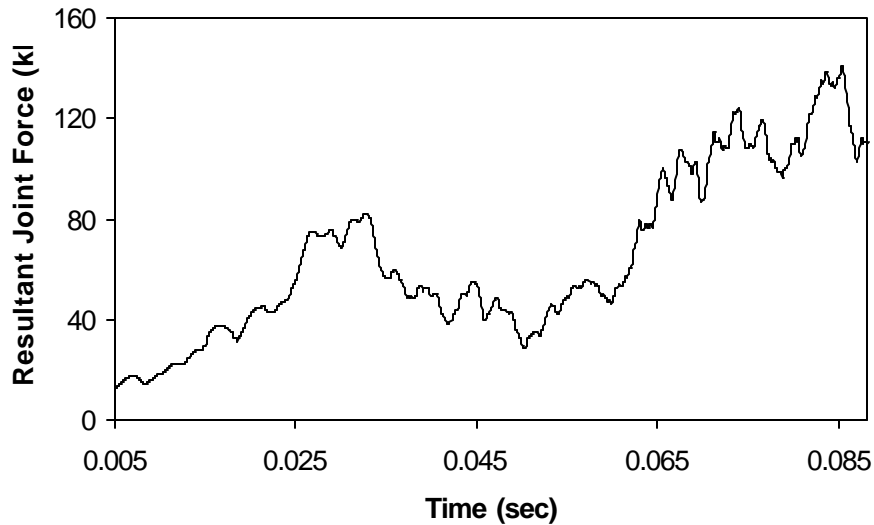


Figure 51. The resultant joint forces versus time for the CRT post (filtered to SAE 60).

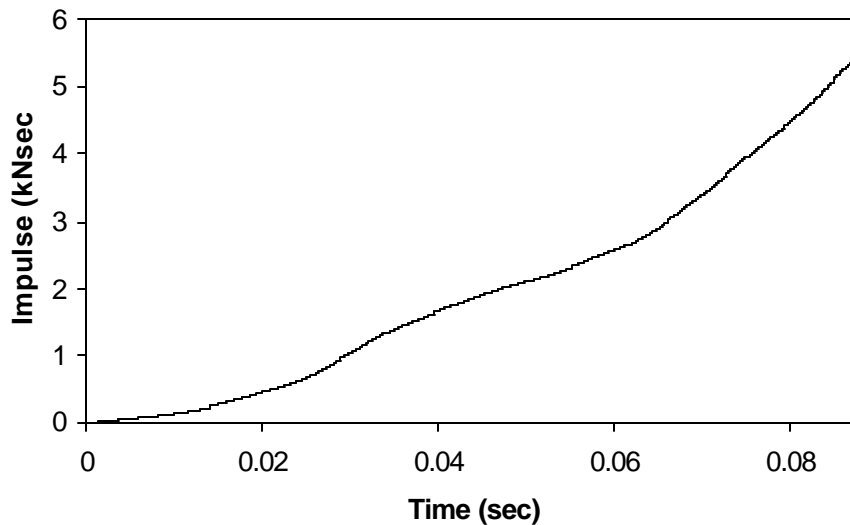


Figure 52. The impulse delivered on the wheel for the CRT post.

The maximum joint force is around 140 kN and the impulse is around 5 kN-sec. Those values on the maximum joint force and impulse are compared to the standard 150x200 mm wood post, where the values were approximately 180 kN and 6 kN-sec respectively. The maximum joint force and impulse for the CRT post is lower than for the standard wood post as expected since the post fails, which reduces the snag potential even though the overlap between the wheel and the post in this case is much larger than in the standard wood post case. The purpose with this model is to show that even though the lateral loading is absent failure caused by the wheel interaction occurs, which Figure 50 shows.

With CRT post as initial geometry a different design was developed. The dimensions and the hole diameter are the same as for the CRT post but the lower hole is removed and the upper hole is moved over the ground line and is now located with its center 50 mm above

ground. The design is shown in Figure 53. The purpose of this design is to make it possible to modify regular wood posts after installation to reduce the snag potential of the post.

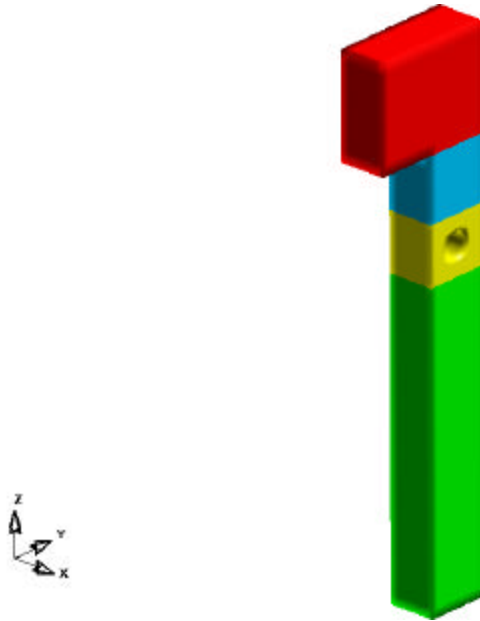


Figure 53. Post with one hole above ground line.

First the post was exposed to lateral loading by the cylindrical impactor and the simulation runtime statistics can be seen in Table 19.

Solid hexahedron elements	4782
Run time	21 hr 8 min
Hardware	IBM
No. of CPU	2
Processor speed	550
Simulated time	0.3 sec

Table 19. Simulation runtime statistics for the post with one hole above ground exposed to wheel contact.

The deflection at ground line is 520 mm and the deflection at guardrail height is 875 mm compared to the standard 150x200 mm where the deflections are approximately 500 mm and 866 mm, respectively. As expected the deflections were similar since this post do not fail because of the lateral loading and should therefore have the same or very similar behavior as the standard 150x200 mm post. The reason for this is the similar mass moment of inertia in the lateral direction of the two posts. In Figures 54 and 55 the contact force between the impactor and the post and the strain energy for the post with one hole above ground line can be seen. Also a comparison with standard 150x200 mm wood post and CRT post can be seen in the figures below.

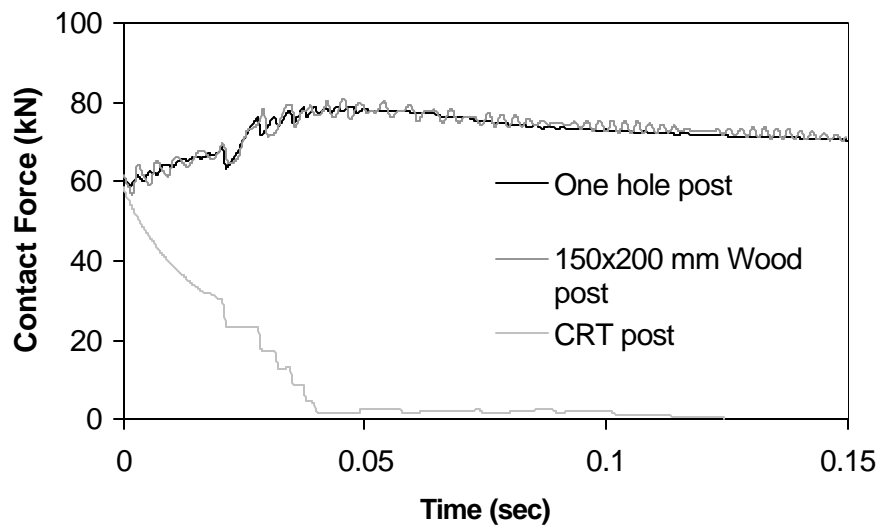


Figure 54. Force time history for the post with one hole above ground bent by cylindrical striker (100 point running average filter).

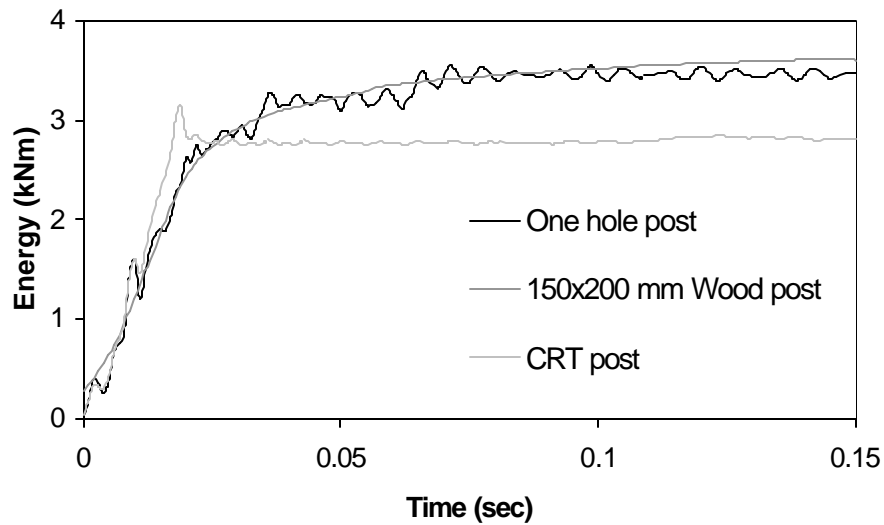


Figure 55. Post strain energy time history for the post with one hole above ground line.

As expected and as can be seen in the figures above the contact force and post strain energy are very similar for the one hole post and the standard 150x200 mm wood post, around 80 kN and 3 kNm. However the curves for the CRT post differ from the one hole post curves since this post fails already at the lateral loading event.

The next step was to assemble the wheel with the vehicle inertia into the model of the post with one hole above ground. For this post the stone wall acting as ground line can be kept in the model since the hole is above ground and the stone wall will therefore not interact with the failure. In this case the post fails partly because of the wheel contact as can be seen in Figure 56.

WHEEL.SR1103
STEP 110 TIME = 2.7248857E-01

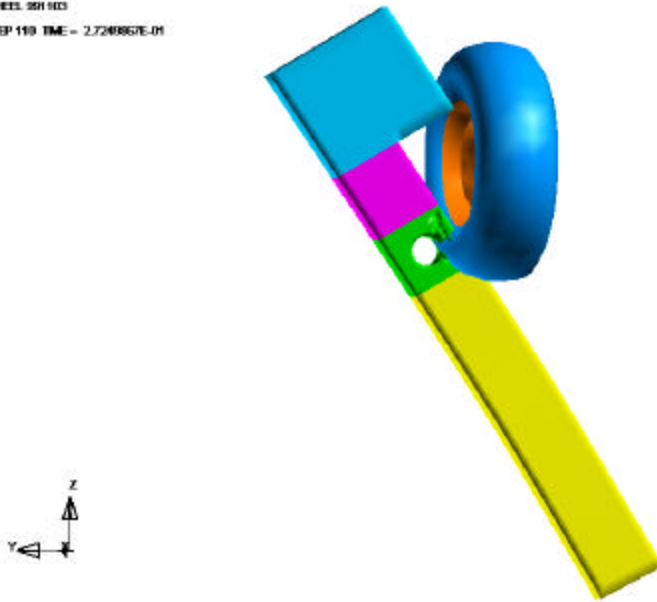


Figure 56. Failure of post with one hole above ground caused by wheel contact.

Simulation runtime statistics for this model are shown in Table 20.

Solid hexahedron elements	5788
Beam elements	4
4-node shell elements	570
Run time	21 hr 5 min
Hardware	IBM
No. of CPU	2
Processor speed	550
Simulated time	0.30 sec

Table 20. Simulation runtime statistics for the post modeled with one hole above ground wheel with vehicle inertia.

The post does not fail completely but the occurred failure is enough to reduce the joint force on the wheel during contact compared to the standard 150x200 mm wood post as can be seen in Figure 57. In Figure 58 the impulse delivered to the wheel versus time is shown.

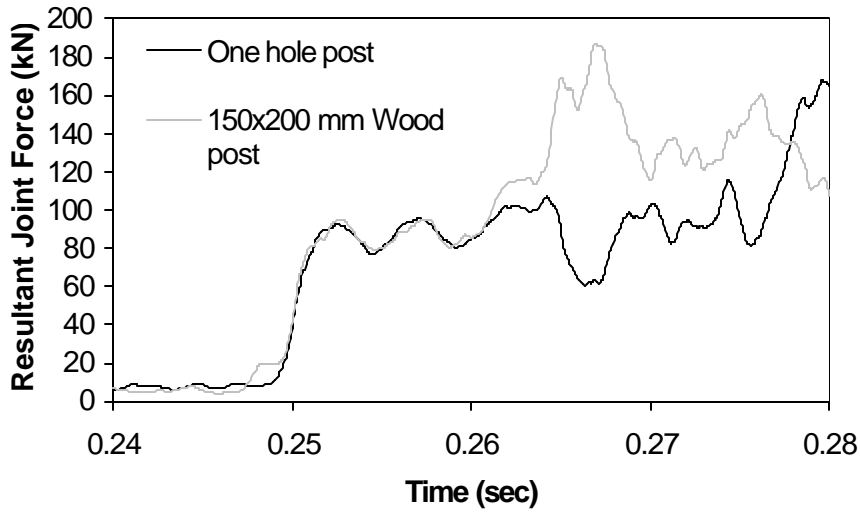


Figure 57. Resultant joint force versus time for the post model with one hole above ground line (filtered to SAE 60).

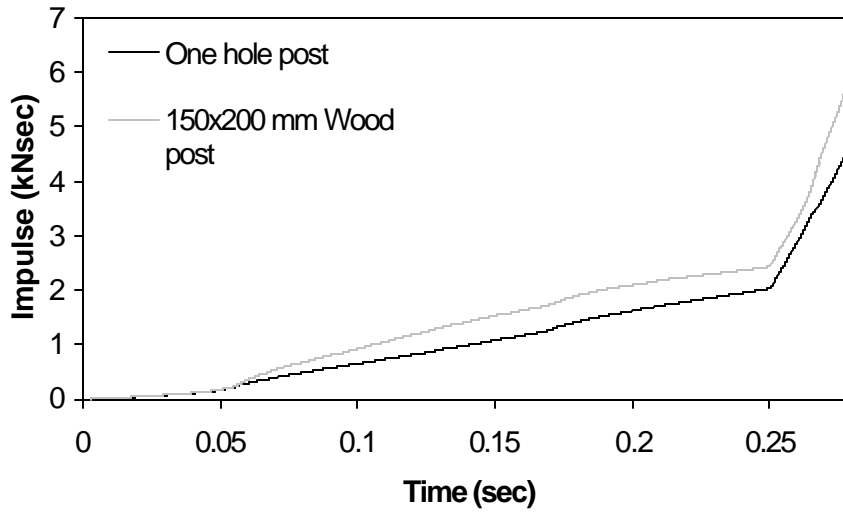


Figure 58. Impulse delivered to the wheel in the model with the post with one hole above ground line.

The maximum joint force is reduced for the one hole post compared to the standard 150x200 mm wood post from around 180 kN to 100 kN after contact occurred. From this

it follows that also the impulse delivered to the wheel is less than for the standard wood post since the impulse corresponds to the area under the joint force curve. The impulse for the one hole post is around 4 kN-sec when contact is ending compared to 6kN-sec for the 150x200 mm wood post.

The results above show that the one hole post does not change in behavior from the standard wood post in the lateral direction but breaks away in the longitudinal direction during a snag.

In Table 21 a comparison between the results in terms of maximum deflection at ground line, maximum joint force and maximum impulse for the standard 150x200 wood post, the CRT post and the one hole post is done.

Post type	Maximum deflection (mm)	Maximum joint force (kN)	Maximum impulse (kN-sec)
150x200 wood post	500	180	6
CRT post	100	140	5
One hole post	520	100	4

Table 21. Comparison between results for the different types of wood posts.

The one hole post is the most advantageous in preventing snagging since it interacts the least with the wheel according to the maximum joint force and impulse values. The CRT post do also have potential in preventing wheel snagging since it usually fails already during the lateral loading event.

8. RESULTS

The FE simulations show wheel snagging in the one-post sub-models for the three investigated standard posts, which agree with full-scale tests found in the crash test literature. A block-out depth of 250 mm on a standard 150x200 mm wood post prevents wheel snagging and a block-out depth of at least 200 mm greatly reduces the snag potential of the wood post. This has not been validated with full-scale crash tests since there are no tests performed on this type of design.

According to FE simulations also the existing CRT post can be used in attempt to prevent wheel snagging since the post fails already during the lateral loading event. A post with the same dimensions as the CRT post but designed with only one hole with diameter 90 mm and center 50 mm above ground line reduces the severity of wheel snagging since the post partly fails during wheel contact, which makes it easier for the wheel to pass.

9. CONCLUSIONS

To prevent snagging on a 150x200 mm wood post designed with a deeper block-out than the standard block-out of 190 mm a block-out depth of 250 mm is required. The results show that for a block-out depth between 100 and 200 mm the performance of the post is not noticeably improved and therefore a post with a block-out depth of at least 200 mm is required to reduce wheel snagging. It appears that the vehicle suspension fails when the joint force reaches a value of 180 kN which correspond to an impulse of 2 kN-sec which are the results for a standard block-out depth of 190 mm. This conclusion can be drawn since full-scale tests have been performed on guardrail systems using standard wood posts with 190 mm block-out where the wheel has been separated from the vehicle after snagging.

Longitudinal fuses are also effective in preventing or reducing wheel snagging. The already existing CRT post prevents wheel snagging according to FE simulations performed. The post fails already during the lateral loading event and will therefore not make an obstacle for the wheel when the wheel contact event starts. A post similar to the CRT post was also developed. This post has one 90 mm diameter hole located with the center 50 mm above ground, which makes it easy to redesign the post after installation. The snag potential for this post turned out to be minor since the post partly fails which decreases the joint forces from a maximum around 180 kNm for the standard 150x200 mm wood post to around 100 kNm, which correspond to maximum impulses of 6 kN-sec and 4 kN-sec respectively. Neither of the results for the posts with longitudinal fuses can

be validated with full-scale tests since there are no such test performed for these types of posts.

Future work, as mentioned earlier in the report, can be to further investigate the effect of longitudinal fuses and also investigate how lateral fuses and different cross-sections can effect the potential of wheel snagging for a post.

This research shows the advantages in using finite element simulations since it saves the time and money that it takes to make full-scale tests. It has also advantages in predicting the course of event that could take place in a full-scale test and therefore make it possible to prevent undesired occurrences in a full-scale test. A finite element simulation gives a lot of detailed data and can therefore also be useful after an unsuccessful full-scale test to discover what went wrong.

10. REFERENCES

1. "TrueGrid Manual", Version 1.4.0, XYZ Scientific Applications, Inc. (June 1998)
2. "LS-DYNA User's Manual", Version 940, Livermore Software Technology Corporation (June 1997)
3. Ivey, D. L., R. Robertson and C. E. Buth, "Test and evaluation of W-beam and thrie-beam guardrails", Report FHWA/RD-82/071, Texas Transportation Institute, Texas A&M University, College Station (March 1986).
4. Stout, D., J. Hinch and T-L Yang, "Force-deflection characteristics of guardrail posts", Report FHWA-88-193, FHWA, US Department of Transportation (September 1988).
5. Mak, K. K. and D. C. Alberson, "Test report NO. 7147-22", Texas Transportation Institute, Texas A&M University, College Station (January 1994).
6. Mak, K. K. and W. C. Menges, "Crash testing and evaluation of strong-post, W-beam guardrail system", Texas Transportation Institute, Texas A&M University, College Station (June 1994).
7. Mak, K. K. and W. C. Menges, "Crash testing and evaluation of modified thrie-beam guardrail system", Texas Transportation Institute, Texas A&M University, College Station (February 1995).
8. Mak, K. K. and W. C. Menges, "Crash testing and evaluation of thrie-beam (G9) guardrail system", Texas Transportation Institute, Texas A&M University, College Station (May 1995).

9. Ray, M. H. and G. S. Patzner, "Finite-element model of modified eccentric loader terminal (MELT)", In Transportation Research record 1599, p.p. 11-21, TRB, National Research Council, Washington D.C. (1997).
10. Plaxico, C. A., G. S. Patzner and M. H. Ray, "Finite-element modeling of guardrail timber posts and the post-soil interaction", In Transportation Research Record 1647, p.p.139-146 (1998).
11. Plaxico, C. A., G. S. Patzner and M. H. Ray, "Effects of post and soil strength on the performance of the modified eccentric loader breakaway cable terminal (MELT)" (1999).
12. Plaxico, C. A., M. H. Ray and K. Hiranmayee, "Comparison of the impact performance of the G4(1W) and G4(2W) guardrail systems under NCHRP report 350 test 3-11 conditions" (2000).
13. Sickling, D. L. and H. E. Ross Jr., "Structural optimization of strong-post W-beam guardrail", In Transportation research record 1133, p.p. 42-50, Transportation Research Board, Washington D.C. (1987).
14. Coon, B. A., J. D. Reid and J. R. Rohde, "Dynamic Impact Testing of Guardrail Posts Embedded in Soil", Midwest Roadside Safety Facility (MwRSF), University of Nebraska-Lincoln (July 1999).
15. Holloway, J. C., M. G. Bierman, B. G. Pfeifer, B. T. Rosson and D. L. Sicking, "Performance Evaluation of KDOT W-Beam Systems", Midwest Roadside Safety Facility (MwRSF), University of Nebraska-Lincoln (May 1996).